

# Additional Massive Binaries in the Cygnus OB2 Association

Daniel C. Kiminki<sup>1,2</sup>, Henry A. Kobulnicky<sup>1</sup>, Ian Ewing<sup>1</sup>, Megan M. Bagley Kiminki<sup>2</sup>, Michael Lundquist<sup>1</sup>, Michael Alexander<sup>1</sup>, Carlos Vargas-Alvarez<sup>1</sup>, Heather Choi<sup>1</sup>, & C. B. Henderson<sup>3</sup>

## ABSTRACT

We report the discovery and orbital solutions for two new OB binaries in the Cygnus OB2 Association, MT311 (B2V + B3V) and MT605 (B0.5V + B2.5V). We also identify the system MT429 as a probable triple system consisting of a tight eclipsing 2.97 day B3V+B6V pair and a B0V at a projected separation of 138 AU. We further provide the first spectroscopic orbital solutions to the eclipsing, double-lined, O-star binary MT696 (O9.5V + B1:V), the double-lined, early B binary MT720 (B0-1V + B1-2V), and the double-lined, O-star binary MT771 (O7V + O9V). These systems exhibit orbital periods between 1.5 days and 12.3 days, with the majority having  $P < 6$  days. The two new binary discoveries and six spectroscopic solutions bring the total number of known massive binaries in the central region of the Cygnus OB2 Association to 20, with all but two having full orbital solutions.

*Subject headings:* techniques: radial velocities — binaries: general — (stars:) binaries: spectroscopic — (stars:) binaries: (*including multiple*) close — stars: early-type — stars: kinematics — surveys

## 1. Introduction

The ubiquity of close massive binaries in open clusters is becoming well documented (e.g., Sana et al. 2009, Mahy et al. 2009, Sana et al. 2008, and De Becker et al. 2006). However, the number of orbital solutions for massive binaries is still relatively small. In our previous works documenting the number and statistics of massive binaries in Cygnus OB2 (Kiminki et al. 2007, 2008, 2009), we discovered nine systems (MT059, MT145, MT252,

---

<sup>1</sup>Dept. of Physics & Astronomy, University of Wyoming, Laramie, WY 82070

<sup>2</sup>Dept. of Astronomy, University of Arizona, Tucson, AZ 85721

<sup>3</sup>Dept. of Astronomy, Ohio State University, Columbus, OH 43210

MT258, MT372, MT720, MT771, Schulte 3, and Schulte 73; notation from Massey & Thompson 1991 and Schulte 1956). We provided spectroscopic solutions to these nine and two additional systems (A36 and A45; notation from Comerón et al. 2002) as part of our ongoing radial velocity survey in one of the Galaxy’s super OB clusters. The primary objective of the Cyg OB2 radial velocity survey is to aid our understanding of numerous open questions involving massive stars, including their formation, the predicted rates of supernovae type Ib/c arising through binary channels, and whether there is a correlation between cluster density and the binary fraction therein.

In this work, we report discovery of two new double-lined spectroscopic binaries (SB2s), and we provide full orbital solutions (periods, mass ratios, eccentricities and probable inclinations) for these and four known binaries previously lacking full solutions. This brings the number of massive binaries having full or partial solutions to 20, the most of any single cluster or association. In a companion paper (Kiminki & Kobulnicky 2012), we summarize the current state of massive binaries in the literature and use the combined binary orbital parameter information and ephemerides for 113 massive stars in Cyg OB2 to infer the intrinsic orbital parameter distributions and the binary fraction of the Association. We present these findings as a complement to analyses of massive stars in other clusters (such as the work with Sco OB2 by Kouwenhoven 2007, NGC 6231 by Sana et al. 2008, NGC 2244 by Mahy et al. 2009, and NGC 6611 by Sana et al. 2009). For a more comprehensive discussion of the scope of this project see Kiminki & Kobulnicky (2012).

Section 2 reviews the observations of this ongoing 12-year radial velocity survey and discusses the method we used to determine radial velocities. Section 3 discusses the method for computing orbital solutions and provides new spectroscopic orbital solutions for MT311, MT429, MT605, MT696, MT720, and MT771. Finally, Section 4 summarizes the survey findings to date.

## 2. Observations and Radial Velocity Measurements

Papers I–III (Kiminki et al. 2007, Kiminki et al. 2008, and Kiminki et al. 2009 respectively) detail the observations of this survey through 2008 October (see Table 1 of Paper III). Since then, we have obtained eleven additional datasets with the WIRO-Longslit spectrograph on the Wyoming Infrared Observatory (WIRO) 2.3 m telescope. The observation dates, including Heliocentric Julian Dates, for these datasets are listed in Table 1. We used the 1800 l mm<sup>-1</sup> grating in first order and obtained a typical spectral resolution of  $\sim 1.5$  Å FWHM across the chip. These observations took place over 26 nights between 2008 December 17 and 2010 October 27 to primarily examine the H $\alpha$ , He I, and He II absorption

lines in suspected SB2s. Exposure times for all observations varied from 300 s to 4500 s (in multiples of 300–900 s) depending on weather conditions and yielded a maximum signal-to-noise ratio (S/N) of 200:1 for the brightest stars. The spectral coverage was 5250–6750 Å. Copper-Argon lamp exposures were taken after each star exposure to wavelength calibrate the spectra to an rms of 0.03 Å (1.4 km s<sup>-1</sup> at 6400 Å). Spectra were Doppler corrected to the heliocentric frame. All new datasets were reduced using standard IRAF<sup>1</sup> reduction routines as outlined in Paper I.

We obtained radial velocities for the single-lined spectroscopic binary (SB1), MT429 via the IRAF cross-correlation task XCSAO in the RVSAO package (Kurtz et al. 1992), using a model stellar atmosphere (Lanz & Hubeny 2003, TLUSTY) of the appropriate effective temperature and gravity (Paper I). Wavelength regions used include  $\lambda\lambda 4020\text{--}4500$  Å (excluding the DIB at  $\lambda 4428$  Å) for the WIYN spectra,  $\lambda\lambda 5250\text{--}6750$  Å (excluding all regions except He II  $\lambda 5411$  Å, He I  $\lambda\lambda 5876, 6678$  Å, and H $\alpha$ ) for the 2008 and 2009 WIRO data, and  $\lambda\lambda 4200\text{--}6000$  Å (excluding the DIB at  $\lambda 4428$  Å) for the 2010 WIRO data. Kurtz et al. (1992) calculate the uncertainties within the XCSAO task as

$$\sigma_v = \frac{3w}{8(1+r)}, \quad (1)$$

a function of the  $r$  statistic (the ratio of the correlation peak height to the amplitude of antisymmetric noise) derived in Tonry & Davis (1979).  $w$  in this equation is the FWHM of the correlation peak.

In order to measure radial velocities for the SB2s, we fit multiple Gaussians to the He I  $\lambda\lambda 5876, 6678$  Å and H $\alpha$  lines. We obtain rough fits to the most deblended (and highest S/N) spectra using the SPLOT routine in IRAF. These values are then used to fit two four-parameter Gaussians simultaneously to those same spectra using the IDL multiple Gaussian fitting routine ARM\_MULTGAUSS (written by Andrew R. Marble at the University of Arizona), which makes use of the non-linear, least-squares, curve fitting IDL package MPFIT (Markwardt 2009). We then adopt the average of the Gaussian widths and depths as fixed parameters to fit line centers for all deblended spectra of the system. The radial velocities are then calculated from the best-fit Gaussian centers. Gaussian parameter uncertainties are obtained from the square-root of the diagonal elements of the covariance matrix multiplied by the measured  $\chi^2$  of the fit. The overall radial velocity uncertainties are obtained by

---

<sup>1</sup>IRAF is distributed by the National Optical Astronomy Observatories, which are operated by the Association of Universities for Research in Astronomy, Inc., under cooperative agreement with the National Science Foundation.

summing the uncertainties on the line centers in quadrature with the typical uncertainty in the wavelength calibration ( $1.4 \text{ km s}^{-1}$  for WIRO and  $2 \text{ km s}^{-1}$  for WIYN). The wavelength solutions of the WIRO-Longslit spectra have been adjusted to a common zero point using the mean of the measured radial velocities of the interstellar Na I  $\lambda\lambda 5889.95, 5895.92 \text{ \AA}$  lines, which we assume are invariant for a given star. WIYN and Keck spectra have been calibrated using radial velocity standard stars (Kiminki et al. 2007, 2008).

### 3. Spectroscopic Solutions

To estimate the periods from the radial velocity data for both the SB1s and SB2s, we analyze the power spectrum as filtered through the CLEAN deconvolution algorithm of Roberts et al. (1987). For computation of the orbital solutions we used the Binary Star Combined Solution Package (referred to as BSCSP in this work) of Gudehus (2001) which makes use of a nonlinear, least-squares subroutine (NONLINFIT) to solve for orbital parameters of binary (SB1 and SB2) and multiple systems using spectroscopic and/or astrometric data. As an added check, we also computed single-component spectroscopic solutions with the least-squares, curve fitting program SBCM (Morbey & Brosterhus 1974) and combined component solutions with SBTWOS, our own MATLAB-based orbital solution program utilizing Markov-Chain Monte Carlo techniques. Solutions from all programs were in good agreement, but BSCSP and SBTWOS yielded orbital parameter uncertainties up to three times larger than those from SBCM. In this work, we present the results with the more conservative uncertainties from BSCSP. For the eclipsing, spectroscopic, triple system MT429, we also used PHOEBE (Prša & Zwitter 2005), an eclipsing binary modeling program based on the code of Wilson & Devinney (1971). PHOEBE provides orbital solutions for eclipsing binary systems with photometric and/or spectroscopic data.

#### 3.1. MT311

At  $V \sim 14$ , the SB2 MT311 is among the faintest in our sample, and the resulting spectra have an average signal-to-noise ratio (S/N) of  $\sim 60$ . The primary is classified a B2V by Massey & Thompson (1991). Given the lower S/N and velocity separation of  $\sim 210 \text{ km s}^{-1}$ , we can only determine approximate spectral types for the components. An absence of He II and relatively strong He I places both components in the early B range. The 2001 August 24 spectrum, obtained at WIYN, shows weak Mg II  $\lambda 4481 \text{ \AA}$  and absent or weak silicon, nitrogen, and carbon (i.e., C III  $\lambda 4070 \text{ \AA}$ , C II  $\lambda 4267 \text{ \AA}$ , Si IV  $\lambda\lambda 4089, 4116 \text{ \AA}$ , Si II  $\lambda\lambda 4128, 4130 \text{ \AA}$ , O II  $\lambda\lambda 4415, 4417 \text{ \AA}$ , N II  $\lambda 3995 \text{ \AA}$ ). This suggests that both components are likely still on

the main sequence. The temperature-sensitive ratio He I  $\lambda 4471 \text{ \AA}$ :Mg II  $\lambda 4481 \text{ \AA}$  indicates an approximate temperature class of B2–B3 for both components. Figure 1 shows the similarity between the line depths for He I  $\lambda 5876 \text{ \AA}$ , H $\alpha$ , and He I  $\lambda 6678 \text{ \AA}$ , suggesting similar luminosities and providing additional support for comparable temperature classes. We, therefore, tentatively classify the components a B2V and a B3V. In Figure 2, we show the 2001 August 24 spectrum of MT311 obtained at WIYN (top). We provide a composite spectrum below MT311, composed of HD42401 (B2V) and HD74280 (B3V) from Walborn & Fitzpatrick (1990). HD42401 and HD74280 have been shifted to the appropriate component radial velocities from Table 2 and scaled to the appropriate luminosity ratio for a B2V and B3V. The MT311 spectrum is smoothed to approximately the resolution of the Walborn & Fitzpatrick (1990) spectra. The stronger absorption present in the He I  $\lambda 4471 \text{ \AA}$  and Mg II  $\lambda 4481 \text{ \AA}$  lines in the MT311 spectrum may be a normalization effect given that the lines fall near the end of the chip. The remaining lines are consistent with the composite spectrum.

Table 2 contains the ephemeris for this system, including radial velocities for the 11 highest S/N spectra. The majority of the spectra were obtained from 2009 June 27 through 2009 September 4 with the Wyoming Infrared Observatory (WIRO) Longslit spectrograph. One observation is from 2001 with the WIYN<sup>2</sup> 3.5 m telescope and Hydra spectrograph. With these 11 spectra, covering a span of eight years, we calculate radial velocities from the He I  $\lambda 5876 \text{ \AA}$  line (He I  $\lambda 4471 \text{ \AA}$  line for the WIYN spectrum) and obtain a period of 5.75 days from the power spectrum for both components with no significant aliases. The best orbital solution, displayed in Figure 3, yields a period of  $P = 5.752 \pm 0.005$  days with a fixed eccentricity of zero. Allowing the eccentricity to vary results in an insignificant decrease in the rms of the fit and yields  $e = 0.22 \pm 0.05$ . Given that the 11 data points do not provide a strong constraint on the eccentricity, we adopt the solution with the fixed zero eccentricity. In the figure, solid symbols correspond to the radial velocities of the primary, open symbols correspond to the radial velocities of the secondary, and the different shapes represent the different instruments/observatories (i.e, squares represent observations taken with WIRO-Longslit and triangles represent observations taken with Hydra at WIYN). We found it more difficult to fit the secondary’s spectral features owing to the low S/N and heavy blending of profiles and thus only utilized 10 measurements (the measurement at  $\phi = 0.808$  was excluded). With a period of  $P = 5.752 \pm 0.005$  days, an eccentricity of  $e = 0.0$ , and semi-amplitudes of  $K_1 = 88 \pm 5 \text{ km s}^{-1}$  and  $K_2 = 118 \pm 9 \text{ km s}^{-1}$ , we calculate masses of  $M_1 \sin^3 i = 3.0 \pm 0.7 M_\odot$  and  $M_2 \sin^3 i = 2.2 \pm 0.4 M_\odot$ , and semimajor axes of  $a_1 \sin i = 10.0 \pm 0.6 R_\odot$  and  $a_2 \sin i = 13.40 \pm 0.01 R_\odot$ . This yields a mass ratio of

---

<sup>2</sup>The WIYN Observatory is a joint facility of the University of Wisconsin, Indiana University, Yale University, and the National Optical Astronomy Observatory.

$q = 0.75 \pm 0.07$  and is consistent with the theoretical mass ratio of  $q = 0.76$  for a B2V+B3V system (Drilling & Landolt 2000). The calculated lower limit masses indicate that the system needs to be inclined at  $i \sim 42^\circ$  to be consistent with the theoretical masses of  $10 M_\odot$  and  $7.6 M_\odot$  for a B2V star and B3V star (Drilling & Landolt 2000).

The computed heliocentric systemic velocity for MT311 is  $\gamma = 1 \pm 4 \text{ km s}^{-1}$ . This differs by nearly  $11 \text{ km s}^{-1}$  from the average systemic velocity of  $-10.3 \text{ km s}^{-1}$  for other members of the Association (Paper I), calling into question its membership. If we adopt an apparent  $V$  magnitude of 13.87 (Massey & Thompson 1991) for the system, the B-V color of 1.39 for the system (Massey & Thompson 1991), an absolute  $V$  magnitudes of -2.45 and -1.94 for a B2V and B3V respectively (Humphreys & McElroy 1984), an intrinsic color  $(B - V)_0 = -0.21$  and a reddening law with  $R_V=3.0$ , the resulting spectrophotometric distance to MT311 is  $\sim 2.6 \text{ kpc}$  (distance modulus of 12.07). The accepted distance to Cyg OB2 is near  $1.7 \text{ kpc}$  (Hanson 2003) but with a relatively large uncertainty owing to the uncertainty on absolute magnitudes for massive stars and the observed variability in the total-to-selective extinction,  $R_V$  (Patriarchi et al. 2003). Although our computed spectrophotometric distance is 50% larger than the accepted distance to Cyg OB2, the uncertainties are sufficiently large that we cannot draw a definitive conclusion regarding the membership of MT311.

Table 2 provides the ephemerides for MT311, MT605, MT696, MT720, and MT771, listing the date (HJD–2,400,000), phase ( $\phi$ ), measured radial velocities ( $V_{r1}$  and  $V_{r2}$ ), and observed minus calculated velocities ( $O_1 - C_1$  and  $O_2 - C_2$ ). Error estimates are shown in parentheses. The complete list of orbital elements and physical parameters for MT311, MT429, MT605, MT696, MT720, and MT771 appears in Table 3. Listed within the table are the period in days ( $P$ ), eccentricity of the orbit ( $e$ ), longitude of periastron in degrees ( $\omega$ ), systemic radial velocity ( $\gamma$ ), epoch of periastron ( $T_0$ ), primary and secondary semi-amplitudes ( $K_1$  &  $K_2$ ), adopted or calculated minimum primary and secondary masses in solar masses ( $M_1$  &  $M_2$ ), primary and secondary mass functions in solar masses ( $f(m)_1$  &  $f(m)_2$ ), spectral classifications from this survey (S.C.<sub>1</sub> & S.C.<sub>2</sub>), the minimum primary and secondary semi-major axes in solar radii ( $a_1 \sin i$  &  $a_2 \sin i$ ), and finally, the rms of the best fitting orbital solution ( $rms_1$  &  $rms_2$ ). Additionally, the inclination, primary and secondary effective temperatures, and component stellar radii are included for MT429.

### 3.2. MT429

Massey & Thompson (1991) classify MT429 ( $\equiv$ V2186 Cyg) as a B0V. Pigulski & Kolaczkowski (1998) showed that this is an eclipsing system of the Algol type, estimating a period of 2.9788 days based on an incomplete light curve. Our spectra of MT429 initially suggested it to be

an SB1 with low-amplitude radial velocity variations at a very similar period.

Figure 4 shows a slightly smoothed, high quality spectrum of MT429, obtained 2001 September 8, with O9V (HD46202), B0V (HD36512), and B1V (HD144470) spectra from the digital atlas of Walborn & Fitzpatrick (1990) for comparison. With the exception of the lower S/N 2000 September 18 Keck spectrum, our spectra of MT429 do not cover the important Si III  $\lambda 4552$  Å line, used with the Si IV  $\lambda 4089$  Å line and the Si II  $\lambda\lambda 4128$ – $4130$  Å lines as the primary temperature class indicator in early B stars. However, the WIYN spectrum in the figure shows a moderately weak Si IV  $\lambda 4089$  Å line and a moderately strong C III + O II blend at  $\lambda\lambda 4070$  Å. These lines quickly diminish with decreasing temperature in early B stars (Walborn & Fitzpatrick 1990). There is also no evidence for He II  $\lambda 4200$ . This agrees with a temperature class of B0–B1. The primary luminosity indicator (Si IV  $\lambda\lambda 4089, 4116$  Å to the nearby He I lines) also agrees with a V luminosity class. All of our spectra support the classification of MT429 as B0V, within a fraction of a temperature class, consistent with the Massey & Thompson (1991) classification.

We obtained 16 spectra on MT429 from 2000 September 18 through 2010 October 27, including one at Keck, five at WIRO, and 10 at WIYN. The WIYN spectra were cross-correlated using a wavelength range of  $\lambda\lambda 4020$ – $4500$  Å (excluding the DIB at  $\lambda 4428$  Å). The WIRO 2010 spectra were cross-correlated using a wavelength range of  $\lambda\lambda 4200$ – $6000$  Å (excluding the DIB at  $\lambda 4428$  Å and the interstellar (IS) Na I lines at  $\lambda\lambda 5890, 5895$  Å). The 2008–2009 WIRO spectra were cross-correlated using a wavelength range of  $\lambda\lambda 5400$ – $6700$  Å (excluding all but the He I, He II, and hydrogen lines owing to the large number of IS lines and DIBs in this spectral range). The Keck spectrum was cross-correlated using a wavelength range of  $\lambda\lambda 4050$ – $5200$  Å (excluding the DIB at  $\lambda 4428$  Å)

The strongest peak in the power spectrum corresponds to a period of  $P = 2.9786$  days with no significant aliases, consistent with the photometric periods of Pigulski & Kolaczowski (1998) and Henderson et al. (2011). Allowing all orbital parameters to vary, BSCSP provides an orbital fit with  $P = 2.9785$ ,  $e = 0.24$ ,  $K = 17.7$  km s $^{-1}$ , and rms of 3.0 km s $^{-1}$ . We excluded one outlier from the fit, the 2008 June 15 WIYN measurement ( $V_r = -48$  km s $^{-1}$ ). Fixing the eccentricity at zero provides a comparable fit to the data with a similar rms of (3.4 km s $^{-1}$ ), period of  $P = 2.9786 \pm 0.0001$  days and systemic velocity of  $\gamma = -14 \pm 1$  km s $^{-1}$ . The resulting mass function of  $f(m) = 0.0012 \pm 0.0003$  would suggest that either the secondary is a low-mass star ( $M_1 \sim 0.8 M_\odot$ ) or that the inclination is very small. A small inclination is inconsistent with the observed eclipses. A large inclination coupled with a low-mass companion could conceivably explain the observed radial velocity curve, but such a scenario entails that only primary eclipses would be observed given the vast difference in temperature between a main sequence or evolved  $\sim 1 M_\odot$  secondary and a B0V primary.

However, existing photometric data clearly show both a primary and a secondary eclipse.

We combined the photometric data of Pigulski & Kolaczkowski (1998) with that of Henderson et al. (2011) who also obtained I-band photometry, finding a nearly identical period of 2.9788 days. We adopted an apparent I magnitude of 11.08 based on the mean maximum magnitude from Henderson et al. (2011). There are 3,710 days between the end of the Pigulski & Kolaczkowski (1998) data and the start of the Henderson et al. (2011) data. This necessitates shifting the Henderson et al. (2011) data by phase  $\phi = 0.225$ . This is approximately equal to a 0.0002 day difference in the calculated period but is consistent within the calculated period uncertainty.<sup>3</sup> Figure 5 shows the combined, adjusted photometric data folded at the 2.9786 day spectroscopic period. Open circles denote the Pigulski & Kolaczkowski (1998) data, and the crosses denote the Henderson et al. (2011) data. The data show a primary to secondary eclipse depth of slightly less than 2:1, indicating components with similar temperatures. Adopting the period, eccentricity, epoch of periastron, and longitude of periastron from the spectroscopic solution, the data were best fit with an inclination of  $i = 74.3^\circ$ , mass ratio of  $q = 0.59$ , separation of  $asini = 22.5 R_\odot$ , primary radius of  $R_1 = 5.5 R_\odot$ , secondary radius of  $R_2 = 3.9 R_\odot$ , primary temperature of  $T_1 = 20,900$  K, and secondary temperature of  $T_2 = 15,200$  K. These results are consistent with a B2V primary and B5V secondary Drilling & Landolt (2000). However, the semi-amplitude of  $16 \text{ km s}^{-1}$  measured from the spectroscopic solution does not agree with the predicted  $137 \text{ km s}^{-1}$  primary radial velocity semi-amplitude from PHOEBE.

The seemingly inconsistent conclusions from the light curve analysis (a B2V + B5V eclipsing binary) and the spectroscopic velocity curve analysis (a B0V with a velocity amplitude of  $16 \text{ km s}^{-1}$  implying a very low-mass companion) posed a conundrum until the discovery that MT429 is a close visual double. Cabellero-Nieves et al. (2011) present adaptive-optics K-band images and *HST* fine guidance sensor measurements showing that the MT429 system is a visual double with a separation of  $0''.08$  (138 AU projected separation at a distance of 1.7 kpc). The fainter component, MT429b, is 1.05 mag fainter at V band than MT429a, consistent with an early-to-mid B star and a B0V at a common distance and reddening. *A consistent picture of MT429 emerges if it is actually a triple system consisting of a B0V star (MT429a) separated by at least 138 AU from a tight B2V+B5V binary (MT429b+MT429c) in a 2.9786 day orbit.* Statistically, the small angular separation of  $0''.08$  between the two dominant components in MT429 is improbable unless there is a physical association (Cabellero-Nieves et al. 2011). With this new information, we adjusted the photometric data to remove the additional flux contributed by the B0V, estimated to be  $\sim 72\%$  of

---

<sup>3</sup>The radial velocity data also required a phase shift amounting to 0.09 after 1,137 days, which is equivalent to a period difference of  $\sim 0.0002$  days and consistent within our calculated orbital period uncertainty.

the total flux by Cabellero-Nieves et al. (2011). Because a larger percentage of the total light is being eclipsed with the B0V flux subtracted, the eclipse depths appear deeper compared to the light curve in Figure 5. The upper panel in Figure 6 shows the adjusted, combined photometric data with the new PHOEBE fit. Again, adopting the period, eccentricity, epoch of periastron, and longitude of periastron from the spectroscopic solution, the best fit to the data results in an inclination of  $i = 89^\circ$ , mass ratio of  $q = 0.68$ , separation of  $asin i = 20.4 R_\odot$ , primary radius of  $R_1 = 4.8 R_\odot$ , secondary radius of  $R_2 = 3.6 R_\odot$ , primary temperature of  $T_1 = 19,100$  K, and secondary temperature of  $T_2 = 13,700$  K. This is most consistent with a B3V primary and B6V secondary (Drilling & Landolt 2000). The new result predicts a radial velocity primary semiamplitude of  $\sim 140$  km s $^{-1}$  (205 km s $^{-1}$  for the secondary), still in sharp disagreement with the measured semiamplitude of 16 km s $^{-1}$ . The lower panel of Figure 6 shows the theoretical velocity curves of the B3V (solid curve) and B6V (dashed curve) stars prescribed by the above scenario. We believe the answer to this discrepancy lies in the fact that the B3V is roughly 5.5 $\times$  fainter than the B0V and the B6V is significantly fainter than the B3V in the visual band, and the large velocity amplitude of the tight binary is masked (spectral dilution) by the much brighter (apparently) constant-velocity B0V component MT429a. Simulations wherein we combine spectra with appropriate flux and signal-to-noise ratios support the conclusion that a 140 km s $^{-1}$  velocity amplitude signal from MT429b is diluted to the level of  $\sim 16$  km s $^{-1}$  in a composite B0V+B3V spectrum. The symbols in the lower panel (filled circles for WIRO, triangles for WIYN, a diamond for Keck) show the apparent velocity curve measured in the composite spectrum of the system. The dotted line shows the systemic velocity of the binary ( $\gamma = -14 \pm 1$ ). While the period of the folded velocity data agrees well with the photometric data, the small implied velocity amplitude of 16 km s $^{-1}$  is not representative of the velocity of any component within the system. MT429, then, is the first massive triple system discovered in the CygOB2 radial velocity survey. It joins Schulte 5 and Schulte 8 as a growing group of N>2 multiple-star systems in the Cyg OB2 Association.

We adopt from BSCSP the values and uncertainties pertaining to the orbital period, eccentricity, epoch of periastron, and angle of periastron for the B3V+B6V pair and list these in Table 3. We adopt the values for component radii, masses, effective temperatures, theoretical semiamplitude semimajor axes, and mass ratio from PHOEBE. These pertain to the tight B3V+B6V system. The listed systemic velocity of the system pertains to the composite system. The RV ephemeris for MT429 is listed in Table 4 and includes the date ( $HJD - 2,400,000$ ), phase ( $\phi$ ), measured radial velocity ( $V_r$ ), cross-correlation  $1\sigma$  error ( $1\sigma$  *err*). We reiterate here that, while these velocities show excellent agreement with the period and phase angle derived from the light curve, the *amplitudes* are not physically meaningful, as they reflect the radial motion of the B3V component as diluted by the (apparently

constant velocity) spectrum of the brighter B0V component.

### 3.3. MT605

Massey & Thompson (1991) classify MT605 a B0.5V. In Paper I, we typed the presumed single system a B1V based on visual comparisons with spectra from the Walborn & Fitzpatrick (1990) digital atlas. We now know that this is an SB2. Examination of the highest quality spectra for this system shows that neither component’s spectrum displays any He II, indicating that the components are likely later than B0. However, very weak Mg II  $\lambda 4481 \text{ \AA}$  absorption relative to He I  $\lambda 4471 \text{ \AA}$  indicates the components are earlier than B2. Furthermore, because Si III  $\lambda 4552 \text{ \AA}$  and Si IV  $\lambda 4089 \text{ \AA}$  are also weak and C III+O II  $\lambda \lambda 4070, 4650 \text{ \AA}$  absorption is strong, we reclassify the primary a B0.5V (in agreement with the original assessment of Massey & Thompson 1991) with acknowledgment that the small velocity separation ( $\sim 160 \text{ km s}^{-1}$  for He I) at a resolution of  $R \sim 4500$  makes the luminosity classification difficult and still somewhat uncertain. With a mass ratio near unity and a luminosity ratio also near unity (determined from examination of all lines while in or near quadrature), we also tentatively classify the secondary a B0.5–B1 with an indeterminate luminosity class. Figure 7 displays the 2001 September 9 spectrum of MT605 taken near quadrature (top) and obtained at WIYN and HD36960 (B0.5V) from the Walborn & Fitzpatrick (1990) digital atlas for comparison. The WIYN spectrum has been boxcar smoothed to approximately the resolution of the Walborn & Fitzpatrick (1990) spectra. The comparison spectrum is in good agreement with the WIYN spectrum of MT605, with the exception of the C III+O II  $\lambda \lambda 4070, 4650 \text{ \AA}$  blend and Si IV  $\lambda 4089 \text{ \AA}$  absorptions, which appear slightly stronger in HD36960.

We observed this system 37 times between 1999 and 2009, obtaining 10 spectra (all with WIRO-Longslit) with sufficiently high enough S/N and large enough component profile velocity separations ( $\sim 150 \text{ km s}^{-1}$  at max) to measure radial velocities. Because of the small number of suitable spectra available for measuring radial velocities, determining an estimate of the period from the power spectrum is difficult. We, therefore, fit single Gaussians to the He I  $\lambda 5876 \text{ \AA}$  and  $H\alpha$  lines and measured the profiles’ Gaussian FWHM in 18 of the WIRO spectra (17 for He I  $\lambda 5876 \text{ \AA}$ ). From these measurements, we observe a strong peak in the power spectrum at  $\sim 6$  days for both He I and  $H\alpha$ . This represents half the period of the binary and tells us the location of the primary and secondary spectral features when the profiles are blended. Using this information, we performed the same technique as with the other SB2s to calculate radial velocities from the He I  $\lambda 5876 \text{ \AA}$  line for the 10 spectra. The power spectrum revealed that the likely period from the 10 spectra is 12.26 days for both the

primary and secondary star spectral features. The best orbital solution provided by BSCSP and SBTWOS yields a period of  $P = 12.27 \pm 0.02$  days, an eccentricity of  $e = 0.24 \pm 0.07$ , and semi-amplitudes of  $K_1 = 44 \pm 3$  km s<sup>-1</sup> and  $K_2 = 77 \pm 5$  km s<sup>-1</sup>. This solution is shown with the folded radial velocity curve in Figure 8. The solution also results in masses of  $M_1 \sin^3 i = 1.3 \pm 0.3$  and  $M_2 \sin^3 i = 0.7 \pm 0.1$ , indicating a mass ratio of  $q = 0.57 \pm 0.05$ . This computed mass ratio suggests that the secondary may be 2–3 subclasses later than the primary, and a main-sequence spectral type of B2.5:V would be in better agreement with the observed mass ratio than our original determination of a B1 from analysis of the line profiles alone. In addition, a relatively low inclination of  $i \sim 26^\circ$  would be required for the component masses to be consistent with the theoretical masses of a B0.5V and B2.5V (Drilling & Landolt 2000).

A time series of the 10 spectra used in the analysis, in order of phase, is provided for illustrative purposes in Figure 9. Panel 1 shows the line profiles of He I  $\lambda 5876$  Å panel 2 shows the line profiles of H $\alpha$ , and panel 3 shows the line profiles of He I  $\lambda 6678$  Å.

### 3.4. MT696

Rios & DeGioia-Eastwood (2004) reveal the binary status of this interacting, eclipsing system composed of an O9.5V and an early B star. The authors find a period of  $P = 1.46$  days and present spectra also showing the SB2 nature of the system. We present the first spectroscopic solution for this binary using 17 spectra obtained with WIRO–Longslit from 2008 August 20 through 2008 September 19. Owing to the large profile widths of the He I  $\lambda 5876$  Å lines and a maximum line-velocity separation of  $\sim 550$  km s<sup>-1</sup>, the positively shifted He I  $\lambda 5876$  Å profiles and the interstellar Na I  $\lambda 5890$  Å line are sometimes partially blended. The broad spectral features, present in both components and possibly indicative of large rotational velocities, is shown in Figure 10. The figure presents a time progression of the He I  $\lambda 5876$  Å, H $\alpha$ , and  $\lambda 6678$  Å lines (left, middle, and right panels respectively) in order of phase. Rios & DeGioia-Eastwood (2004) report this system as W UMa type, but the spectra show no evidence of emission lines which are common in contact binaries and systems with accretion disks. Given that this system has such a short period, the possibility that this is (or has been) a contact binary cannot be ruled out, but the early spectral types of the components, the current absence of emission features, and the longer than 1 day period suggest that this may in fact be a Beta Lyr type system instead.

We computed orbital solutions based on both the He I  $\lambda 5876$  Å velocities and H $\alpha$  velocities. The He I and H $\alpha$  spectroscopic periods for both components agreed with Rios & DeGioia-Eastwood (2004) and showed strong signals in the power spectra at  $\sim 1.46$  days. The orbital solu-

tion based on the  $H\alpha$  velocities, illustrated by the solid line in Figure 11, yields a period of  $P = 1.4692 \pm 0.0005$  days, eccentricity of  $e = 0.01 \pm 0.02$ , semi-amplitudes of  $K_1 = 261 \pm 4$  km s $^{-1}$  and  $K_2 = 277 \pm 6$  km s $^{-1}$ , and mass ratio of  $q = 0.94 \pm 0.02$ . The  $H\alpha$  radial velocities are represented by the open (secondary) and filled (primary) circles, and the He I  $\lambda 5876$  Å velocities are represented by open and filled triangles. The orbital solution based on the He I  $\lambda 5876$  Å velocities yields a period of  $P = 1.467 \pm 0.004$  days, eccentricity of  $e = 0.05 \pm 0.02$ , semi-amplitudes of  $K_1 = 261 \pm 6$  km s $^{-1}$  and  $K_2 = 327 \pm 10$  km s $^{-1}$ , and mass ratio of  $q = 0.80 \pm 0.03$ . The period, eccentricity, epoch of periastron, longitude of periastron, and systemic velocities for both solutions showed good agreement. We find a systemic velocity of  $\gamma = -10 \pm 3$ , consistent with other Cyg OB2 members. The secondary semi-amplitudes, however, differ by  $\sim 50$  km s $^{-1}$ . The more positive semi-amplitude of the  $H\alpha$  line may be a result of some interaction between the two stars as  $H\alpha$  is more easily distorted in such scenarios because of its formation higher in the stellar atmosphere or possibly in an extended photosphere/envelope. However, given that the  $H\alpha$  line profiles are high S/N, we adopted the period, eccentricity, systemic velocity, angle of periastron, and epoch of periastron from this solution and fixed them in the determination of a revised He I  $\lambda 5876$  Å solution. This is represented by the dotted line in Figure 11. The ephemerides for both the  $H\alpha$  solution and the combined  $H\alpha$ +He I  $\lambda 5876$  Å solution are provided in Table 2. The orbital elements to the combined  $H\alpha$ +He I  $\lambda 5876$  Å solution are provided in Table 3.

Adopting the revised He I orbital solution, we obtain a mass ratio of  $0.85 \pm 0.03$ . This, coupled with the nearly equal line depths for all features, suggests a secondary spectral type similar to the primary’s. Without the photometric data, we can only speculate on the inclination of MT696. However, assuming a theoretical mass of  $16 \pm 0.5 M_\odot$  for the primary (Martins et al. 2005), the calculated masses ( $M_1 \sin^3 i = 15.1 \pm 0.7 M_\odot$  and  $M_2 \sin^3 i = 12.8 \pm 0.5 M_\odot$ ) suggest that the system has an inclination of near  $80^\circ$  and a secondary with a spectral type of B1V.

### 3.5. MT720

In Paper II, we find that the SB2 MT720 is most likely composed of two early B stars based on the absence of Mg II  $\lambda 4481$  Å and strength of the He I lines. Based on new WIRO-Longslit observations of this system, we agree with our previous assessment. The new spectra show relatively strong He I absorption and no evidence of He II. The paucity of stellar lines in this spectral regime and the low S/N of our spectra still make accurate spectral typing difficult. Figure 12 shows the dominant stellar lines in the 5250–6700 Å regime (He I  $\lambda 5876$  Å,  $H\alpha$ , and He I  $\lambda 6678$  Å) near quadrature. The spectrum is a composite of

seven spectra between  $\phi = 0.5$  and  $\phi = 0.7$ . The line depths and widths are similar and suggest comparable spectral types for the components. In order to draw further conclusions regarding the component spectral types, we examined the following orbital solution and component mass estimates.

We measured radial velocities for 32 of the 35 WIRO-Longslit spectra obtained on MT720 using the He I  $\lambda 5876 \text{ \AA}$  profiles. These 32 radial velocities provide a clear period of 4.36 days from the power spectra of both components. The power spectra also contained no significant aliases. The 4.36 day period agrees with our original visual assessment of just under 5 days in Paper II. The best combined orbital solution obtained from BSCSP produces a period of  $P = 4.3622 \pm 0.0003$  days and an eccentricity of  $e = 0.35 \pm 0.02$ . Figure 13 displays this solution. We note that this solution presents an unusually large eccentricity for such a short-period system. We computed additional solutions with an eccentricity fixed at lower values, but these resulted in a much larger rms ( $\gg 21.6 \text{ km s}^{-1}$  for the primary and  $\gg 29.5 \text{ km s}^{-1}$  for the secondary). Given semi-amplitudes of  $K_1 = 173 \pm 5 \text{ km s}^{-1}$  and  $K_2 = 242 \pm 7 \text{ km s}^{-1}$ , the calculated mass ratio is  $q = 0.71 \pm 0.06$ . Additionally, the calculated minimum masses,  $M_1 \sin^3 i = 15.5 \pm 0.8 M_\odot$  and  $M_2 \sin^3 i = 11.1 \pm 0.6 M_\odot$ , indicate that the likely spectral types of the components are B0–1V and B1–2V for the primary and secondary respectively (interpolated from Drilling & Landolt 2000). There is no record of photometric variability for this system, but if the primary has a B0V or later spectral type, the minimum masses of the components preclude inclinations lower than  $i \sim 70^\circ$ . The remaining orbital parameter values are listed in Table 3.

### 3.6. MT771

The He I lines of the SB2, late O-type binary MT771 show a strong Struve-Sahade effect (for a good summary of this effect, see Linder et al. 2007). This effect causes asymmetries or varying line depth/width and, in the case of MT771, is present in both components' spectra. This makes component identification tricky for such a short period ( $< 3$  days) system, even with a maximum velocity separation of  $\sim 300 \text{ km s}^{-1}$ . The much broader  $H\alpha$  line remains heavily blended even at the largest velocity separation. We used this to our advantage, following the same procedure as with MT605, fitting a single Gaussian profile to the  $H\alpha$  line and measuring the Gaussian FWHM. The period produced by the FWHM measurements is equal to half the binary period. The FWHM measurements yielded a strong signal in the power spectrum corresponding to a period of 1.43 days with no significant aliases. Even with the varying asymmetries in the component He I profiles, we still chose to use the average measured Gaussian width and depth for each component's He I  $\lambda 5876 \text{ \AA}$  line and

fix these values when measuring the radial velocities (assuming a period of  $\sim 2.86$  days). Of the 34 epochs included for MT771 in Table 2, we omitted two observations for the secondary ( $HJD = 2,454,700.85$  &  $2,455,041.67$ ) when the lines were at their most blended state. As was expected, the power spectra for both components showed a clear, strong signal at 2.86 days. The computed orbital solution for this system produces a period of  $P = 2.8635 \pm 0.0002$  days, an eccentricity of  $e = 0.05 \pm 0.03$ , and semi-amplitudes of  $K_1 = 139 \pm 5$  km s $^{-1}$  and  $K_2 = 164 \pm 6$  km s $^{-1}$ . The solution also produces lower limit component masses of  $M_1 \sin^3 i = 4.5 \pm 0.3 M_\odot$  and  $M_2 \sin^3 i = 3.8 \pm 0.2 M_\odot$  and suggests a low inclination of  $i \lesssim 37^\circ$  for this system (the approximate inclination required to yield the mass of a late O star; Martins et al. 2005). This solution and the radial velocity curve, produced from the 34 WIRO-Longslit spectra obtained between 2007 August 28 and 2009 August 3, is shown in Figure 14. The radial velocities measured at  $\phi = 0.8$ – $1.0$  appear systematically more positive, and this likely stems from the strong asymmetries at these epochs. This is more easily seen in Figure 15, which shows a time series of the He I  $\lambda 5876$  Å line in order of phase. Panel 1 contains the line profiles for  $\phi = 0.07$ – $0.45$  and panel 2 contains the line profiles for  $\phi = 0.45$ – $1.00$ . The He I  $\lambda 5876$  Å line of the primary appears much stronger than the secondary at phases of  $\phi = 0.856$ – $0.906$ , and the secondary also appears asymmetric. The ratio of He line depth also appears to change over a small range of phase (e.g.,  $\phi = 0.355$ – $0.387$ ), though less dramatically.

The strong Struve-Sahade effect indicates that there are likely significant irradiation effects in this system, possibly stemming from a shock region between the components’ stellar winds. If so, the shock region is nearer the secondary as the asymmetry is stronger in the secondary’s spectral lines. The asymmetry may be the result of an unresolved emission feature between the component lines and originate from the shock region. The seemingly irregular strength of the emission would indicate varying wind velocities and densities of one or both stars.

The Struve-Sahade effect also makes spectral typing difficult given that the He I and He II lines are crucial to temperature classification in late O stars (e.g., He II  $\lambda 4541$  Å:He I  $\lambda 4471$  Å, He II  $\lambda 4541$  Å:Si III  $\lambda 4552$  Å, and He I  $\lambda 4471$  Å:Mg II  $\lambda 4481$  Å). Our initial classifications of O7V for the primary and O9V for the secondary, however, appear to still be close given the new computed mass ratio of  $q = 0.85 \pm 0.04$ , the moderately strong He II at  $\lambda\lambda 4200, 4542, \text{ and } 5411$  Å, and strong He I.

#### 4. Summary

We present orbital solutions for two new SB2s, MT311 and MT605. We also provide the first spectroscopic solutions to the eclipsing system, MT696, the early B, eclipsing triple SB1, MT429, the early B SB2, MT720, and the late-O SB2, MT771.

Table 5 lists the 20 known OB binaries in Cyg OB2. Column 1 gives the system designations. Column 2 shows the binary types (i.e., eclipsing, SB1, SB2, etc). Column 3 provides the spectral types of the components. The spectral types in square brackets have been determined indirectly from the data (i.e., based on the computed mass ratio rather than the component’s spectrum). Columns 4–6 give the orbital periods, eccentricities, and mass-ratios respectively. Finally, column 7 lists the corresponding surveys responsible for the orbital information. Figure 16 shows the locations of these systems relative to the other OB stars in this survey. There are no apparent clusterings or groups of massive stars, nor are there tendencies of the massive binaries to reside in the center of the Association versus the outskirts. Of the 20, we know reliably the orbital periods of all 20, the orbital eccentricities of 18, and the mass-ratios of all 20 (the mass ratios for the SB1s are actually range estimates based on the range of probable inclinations). There are six SB1s, 14 SB2s, five eclipsing binaries of the Algol type, two eclipsing binaries of the  $\beta$  Lyr type, and one eclipsing binary of the W UMa type. At least five binaries are both spectroscopic and eclipsing systems. In a companion paper (Kiminki & Kobulnicky 2012), we use the orbital parameter information and ephemerides associated with the short period systems ( $P < 26$  days) listed in Table 5, along with the ephemerides of 94 additional OB stars in Cyg OB2, to compute the intrinsic binary orbital parameter distributions (i.e., period, mass ratio, and eccentricity) and intrinsic binary fraction of the cluster.

We would like to acknowledge the time, effort, and thoroughness of our anonymous referee in assisting to make this a much stronger manuscript. We thank the time allocation committees of the Lick, Keck, WIYN, and WIRO observatories for granting us observing time and making this project possible. We are also appreciative to Chris Fryer, Falk Herwig, and Jean-Claude Passy for providing useful discussion on the intriguing system MT429, and Saida Caballero-Nieves for providing a big piece to the MT429 puzzle in the form of her HST data. Additionally, I would like to thank Steward Observatory at the University of Arizona for providing support and resources during my transition from the University of Wyoming and the final stages of this manuscript. And finally, we are thankful for the continued support from the National Science Foundation through Research Experience for Undergraduates (REU) program grant AST 03-53760, through grant AST 03-07778, and through grant AST 09-08239, and the support of the Wyoming NASA Space Grant Consortium through grant

NNG05G165H. *Facilities*: WIRO (), WIYN (), Shane (), Keck:I ()

## REFERENCES

- Caballero-Nieves, S. M., Gies, D. R., Roberts, L. C., & Turner, N. H. 2011, *Bulletin Société des Sciences de Liège*, 80, 639
- Comerón, F., et al. 2002, *A&A*, 389, 874
- Contreras, M. E., Rodriguez, L. F., Tapia, M., Cardini, D., Emanuele, A., Badiali, M., & Persi, P. 1997, *ApJ*, 488, 153
- De Becker, M., Rauw, G., & Manfroid, J. 2004, *A&A*, 424, L39
- De Becker, M., Rauw, G., Manfroid, J., & Eenens, P. 2006, *A&A*, 456, 1121
- Drilling, J. S., & Landolt, A. U. 2000, in *Astrophysical Quantities*, ed. A. N. Cox (4th ed.; New York: Springer), 381
- Gudehus, D. H. 2001, *BAAS*, 33, 850
- Hall, D. S. 1974, *AcA*, 24, 69
- Hanson, M. M. 2003, *ApJ*, 597, 957
- Henderson, C. B., Stanek, K. Z., & Prieto, J. L. 2011, *ApJ*, 194, 27
- Humphreys, R. M., & McElroy, D. B. 1984, *ApJ*, 284, 565
- Kiminki, D. C., et al. 2007, *ApJ*, 664, 1120
- Kiminki, D. C., Kobulnicky, H. A., Gilbert, I., Bird, S., & Chunev, G. 2009, *AJ*, 137, 4608
- Kiminki, D. C., & Kobulnicky, H. A. 2012, submitted
- Kiminki, D. C., & Kobulnicky, H. A. 2012b, in prep
- Kiminki, D. C., McSwain, M. V., & Kobulnicky, H. A. 2008, *ApJ*, 679, 1478
- Kouwenhoven, M. B. N., Brown, A. G. A., Portegies Zwart, S. F., & Kaper, L. 2007, *A&A*, 474, 77

- Kurtz, M. J., Mink, D. J., Wyatt, W. F., Fabricant, D. G., Torres, G., Kriss, G. A., & Tonry, J. L. 1992, in ASP Conf. Ser. 25, *Astronomical Data Analysis Software and Systems I*, ASP Conf. Ser., ed. D. M. Worrall, C. Biemesderfer, & J. Barnes (San Francisco: ASP), 432
- Lanz, T., & Hubeny, I. 2003, *ApJS*, 146, 417
- Linder, N., Rauw, G., Sana, H., De Becker, M., & Gosset, E. 2007, *A&A*, 474, 193
- Mahy, L., Nazé, Y., Rauw, G., Gosset, E., M. De Becker, Sana, H., & Eenens, P. 2009, *A&A*, 502, 937
- Markwardt, C. B. 2009, in ASP Conf. Ser. 411, *Astronomical Data Analysis Software and Systems XVIII*, ed. D. A. Bohlender, D. Durand, & P. Dowler (San Francisco: ASP), 251
- Martins, F., Schaerer, D., & Hillier, D. J. 2005, *A&A*, 436, 1049
- Massey, P., & Thompson, A. B. 1991, *AJ*, 101, 1408
- Miczaika, G. R. 1953, *PASP*, 65, 141
- Morbey, C. L., & Brosterhus, E. B. 1974, *PASP*, 86, 455
- Nazé, Y., De Becker, M., Rauw, G., & Barbieri, C. 2008, *A&A*, 483, 543
- Nazé et al. 2010, *ApJ*, 719, 634
- Otero, S. 2008a, *Open European Journal on Variable Stars*, 83, 1
- Otero, S. 2008b, *Open European Journal on Variable Stars*, 91, 1
- Patriarchi, P., Morbidelli, L., & Perinotto, M. 2003, *A&A*, 410, 905
- Pigulski, A., & Kolaczowski, Z. 1998, *MNRAS*, 298, 753
- Prša, A., & Zwitter, T. 2005, *ApJ*, 628, 426
- Rauw, G., Vreux, J. M., & Bohannan, B. 1999, *ApJ* 517, 416
- Rios, L. Y., & DeGioia-Eastwood, K. 2004, *BAAS*, 205, No. 09.05
- Roberts, D. H., Lehár, J., & Dreher, J. W. 1987, *AJ*, 93, 968
- Romano, G. 1969, *MmSAI*, 40, 375

- Sana, H., Gosset, E., Nazé Y., Rauw, G., & Linder, N. 2008, MNRAS, 386, 447
- Sana, H., Gosset, E., & Evans, C. J. 2009, MNRAS, 400, 1479
- Schulte, D. H. 1956, ApJ, 123, 250
- Stroud, V. E., Clark, J.S., Negueruela, I. , Roche, P., & Norton, A.J. 2009, A&A, 511, 84
- Tonry, J., Davis, M. 1979, AJ, 84, 1511
- Walborn, N. R. 1973, ApJ, 180, L35
- Walborn, N. R., & Fitzpatrick, E. L. 1990, PASP, 102, 379
- Wilson, O. C. 1948, PASP, 60, 385
- Wilson, O. C., & Abt, A. 1951, ApJ, 144, 477
- Wilson, R. E., & Devinney, E. J. 1971, ApJ, 166, 605
- Wozniak, P. R., et al. 2004, AJ, 127, 2436, Northern Sky Variability Survey: Public Data Release

Table 1. Dates of WIRO Observing Runs

Date	Date Coverage (HJD)
2008 Dec 17	2,454,818
2009 Jan 3	2,454,835
2009 Jan 16	2,454,848
2009 Jun 27–30	2,455,010–2,455,013
2009 Jul 5	2,455,018
2009 Jul 27,28	2,455,040–2,455,041
2009 Jul 30–Aug 3	2,455,043–2,455,047
2009 Aug 26–29	2,455,070–2,455,073
2009 Aug 31–Sep 4	2,455,075–2,455,079
2010 Aug 21	2,455,430
2010 Oct 27	2,455,497

Table 2. Ephemerides for MT311, MT696, MT720, & MT771

Date (HJD-2,400,000)	$\phi$	$V_{r1}$ (km s <sup>-1</sup> )	$O_1 - C_1$ (km s <sup>-1</sup> )	$V_{r2}$ (km s <sup>-1</sup> )	$O_2 - C_2$ (km s <sup>-1</sup> )
MT311					
52,146.68.....	0.569	-98.0 (10.5)	-13.2	104.5 (22.4)	-11.9
55,010.64.....	0.457	-87.1 (6.2)	-10.4	101.1 (11.0)	-4.4
55,011.78.....	0.655	-75.7 (6.8)	-12.8	83.8 (12.0)	-3.3
55,012.72.....	0.818	27.2 (6.3)	7.6	-62.3 (11.0)	-39.2
55,013.82.....	0.010	77.8 (4.9)	-10.8	-104.1 (8.5)	11.1
55,070.66.....	0.891	67.5 (6.8)	11.4	-123.3 (11.9)	-51.5
55,071.72.....	0.075	72.7 (4.7)	-14.2	-91.6 (8.4)	21.2
55,076.81.....	0.961	81.6 (6.9)	1.3	-91.6 (12.2)	12.5
55,077.74.....	0.122	86.5 (5.1)	9.9	-104.1 (9.0)	-4.9
55,078.73.....	0.293	20.8 (5.1)	24.3	...	...
55,079.76.....	0.472	-81.6 (5.1)	-1.4	132.3 (9.0)	21.9
MT605					
54,643.87.....	0.241	-52.8 (4.9)	-3.7	65.8 (6.8)	11.8
54,674.94.....	0.776	22.2 (5.1)	-0.8	-64.7 (7.2)	4.4
55,043.65.....	0.837	26.6 (5.9)	-6.3	-75.9 (8.2)	13.3
55,044.75.....	0.926	42.6 (7.2)	5.4	-107.8 (10.0)	-11.1
55,045.68.....	0.003	7.5 (6.3)	-9.7	-58.0 (8.8)	4.0
55,072.64.....	0.204	-47.7 (7.5)	-1.4	38.4 (10.4)	-10.6
55,073.69.....	0.287	-36.3 (7.4)	13.3	49.8 (10.4)	-4.9
55,075.62.....	0.444	-48.0 (6.1)	-10.6	37.8 (8.4)	4.3
55,078.63.....	0.690	7.1 (8.7)	3.5	-31.0 (12.2)	6.9
55,079.68.....	0.776	27.4 (7.7)	6.0	-77.4 (10.7)	-8.3
MT696 (He I $\lambda$ 5876 Å + H $\alpha$ )					
54,699.74.....	0.080	-247.5 (5.2)	9.5	355.0 (7.2)	73.7
54,701.91.....	0.556	298.8 (4.2)	50.3	-305.2 (11.7)	9.0
54,724.62.....	0.012	-266.9 (3.7)	1.0	321.6 (2.8)	27.4
54,724.73.....	0.087	-262.1 (2.9)	-9.4	270.7 (2.4)	-5.7
54,724.82.....	0.153	-170.9 (4.9)	25.3	243.4 (7.9)	33.6
54,725.61.....	0.687	147.9 (2.7)	15.6	-186.4 (5.6)	-9.1
54,725.74.....	0.773	2.8 (12.5)	4.4	-11.9 (4.0)	7.6
54,725.85.....	0.854	-117.4 (4.5)	10.8	153.2 (11.1)	23.6
54,726.63.....	0.381	107.2 (3.3)	-39.0	-242.6 (8.5)	-49.1
54,726.74.....	0.459	217.9 (4.3)	-9.1	-308.9 (15.6)	-20.1
54,726.84.....	0.526	243.2 (1.9)	-9.0	-322.4 (8.0)	-3.8
54,729.63.....	0.423	165.4 (3.8)	-30.5	-283.2 (11.0)	-31.0
54,729.72.....	0.488	241.8 (3.0)	-1.7	-324.9 (11.2)	-16.6
54,729.81.....	0.548	264.5 (4.5)	14.3	-312.1 (9.8)	4.2

Table 2—Continued

Date (HJD-2,400,000)	$\phi$	$V_{r1}$ (km s <sup>-1</sup> )	$O_1 - C_1$ (km s <sup>-1</sup> )	$V_{r2}$ (km s <sup>-1</sup> )	$O_2 - C_2$ (km s <sup>-1</sup> )
MT696 (H $\alpha$ )					
54,699.74.....	0.079	-242.9 (4.7)	14.4	282.5 (12.3)	29.4
54,700.77.....	0.781	9.3 (6.0)	22.6	10.1 (10.4)	16.3
54,700.90.....	0.869	-183.5 (6.6)	-33.7	127.6 (7.8)	-11.2
54,701.91.....	0.555	254.1 (4.5)	5.4	-280.3 (6.6)	4.2
54,722.84.....	0.800	19.2 (19.2)	63.2	-32.3 (135.5)	-58.7
54,724.62.....	0.011	-269.9 (5.0)	-2.1	262.2 (7.3)	-2.0
54,724.73.....	0.087	-245.6 (4.8)	7.6	271.5 (11.0)	22.7
54,724.82.....	0.152	-180.7 (5.5)	16.5	197.7 (10.4)	8.5
54,725.61.....	0.686	160.3 (12.5)	26.8	-123.6 (12.9)	38.5
54,725.74.....	0.773	7.0 (13.0)	7.3	25.8 (54.8)	45.8
54,725.85.....	0.853	-145.2 (4.8)	-18.2	109.3 (2.1)	-5.4
54,726.63.....	0.381	156.7 (8.0)	11.6	-179.2 (11.4)	-4.8
54,726.74.....	0.458	222.5 (4.4)	-3.9	-279.8 (10.3)	-19.0
54,726.84.....	0.526	256.7 (8.7)	4.5	-291.3 (7.7)	-3.0
54,729.63.....	0.423	196.0 (5.8)	1.0	-252.8 (7.8)	-25.3
54,729.72.....	0.487	246.0 (9.5)	2.8	-280.1 (8.8)	-1.4
54,729.81.....	0.548	262.1 (9.5)	11.7	-287.2 (8.8)	-0.8
MT720					
54,341.83.....	0.072	-93.4 (10.5)	0.1	135.0 (14.8)	25.9
54,343.81.....	0.524	149.2 (15.9)	6.9	-228.0 (22.4)	-7.0
54,345.82.....	0.986	-66.8 (14.4)	-14.0	78.2 (20.3)	26.2
54,346.87.....	0.226	-166.8 (15.4)	-19.3	208.6 (21.7)	23.8
54,348.76.....	0.660	163.7 (13.5)	3.0	-216.6 (19.0)	30.4
54,399.56.....	0.306	-171.8 (7.1)	-17.8	180.5 (9.9)	-13.3
54,399.71.....	0.340	-153.4 (7.2)	-7.8	179.2 (10.1)	-2.9
54,401.55.....	0.760	95.8 (7.3)	9.4	-130.8 (10.3)	12.2
54,401.71.....	0.798	83.4 (8.3)	23.5	-96.8 (11.7)	8.9
54,402.62.....	0.006	-79.0 (5.8)	-16.2	76.8 (8.2)	10.8
54,402.75.....	0.036	-76.5 (7.0)	0.6	88.8 (9.8)	2.7
54,405.60.....	0.691	138.9 (9.7)	0.5	-195.5 (13.6)	20.2
54,406.59.....	0.916	-49.4 (7.8)	-34.7	33.9 (11.2)	35.3
54,408.58.....	0.374	-141.9 (9.5)	-15.5	128.2 (13.3)	-26.9
54,409.57.....	0.600	183.0 (9.9)	-7.0	-256.7 (13.9)	31.2
54,409.75.....	0.641	139.6 (9.7)	-32.9	-222.8 (13.7)	40.7
54,410.57.....	0.830	39.2 (7.2)	0.9	-114.3 (10.1)	-39.0
54,410.75.....	0.871	49.2 (11.5)	37.3	-62.2 (16.1)	-23.6
54,643.88.....	0.313	-141.7 (5.6)	11.3	216.9 (8.0)	24.4
54,696.75.....	0.434	-70.8 (6.5)	-23.0	70.9 (9.1)	25.8
54,725.82.....	0.097	-109.8 (8.8)	-5.5	124.1 (12.3)	-0.1
54,748.72.....	0.347	-123.8 (7.8)	18.9	189.0 (11.0)	11.1
54,754.67.....	0.710	106.2 (8.3)	-17.5	-216.7 (11.7)	-21.6

Table 2—Continued

Date (HJD-2,400,000)	$\phi$	$V_{r1}$ (km s <sup>-1</sup> )	$O_1 - C_1$ (km s <sup>-1</sup> )	$V_{r2}$ (km s <sup>-1</sup> )	$O_2 - C_2$ (km s <sup>-1</sup> )
54,755.67.....	0.940	-61.1 (8.9)	-33.1	29.3 (12.5)	11.9
54,757.65.....	0.395	-104.6 (10.7)	1.7	138.7 (15.1)	11.7
55,046.79.....	0.676	117.7 (12.9)	-31.7	-242.5 (18.2)	-11.4
55,070.71.....	0.161	-133.8 (11.6)	-5.1	178.7 (16.3)	20.2
55,071.67.....	0.381	-97.8 (11.9)	22.5	143.1 (16.7)	-3.5
55,072.71.....	0.619	191.5 (10.5)	7.4	-232.0 (14.8)	47.7
55,076.76.....	0.546	174.9 (13.8)	4.2	-249.5 (19.5)	11.5
55,078.66.....	0.982	-66.0 (10.3)	-15.5	109.5 (14.4)	60.6
55,079.71.....	0.223	-141.3 (12.4)	5.5	219.8 (17.4)	36.0
MT771					
54,341.82.....	0.752	-139.3 (8.1)	-38.9	85.1 (9.9)	-5.8
54,342.81.....	0.097	-65.6 (4.0)	-22.7	19.3 (4.9)	-3.7
54,343.82.....	0.449	93.3 (6.9)	-15.4	-181.0 (8.5)	-25.1
54,345.83.....	0.153	6.6 (6.3)	-2.7	-69.2 (7.7)	-30.6
54,347.82.....	0.847	-154.9 (8.8)	-5.0	113.7 (10.8)	-35.7
54,348.77.....	0.179	23.7 (5.2)	-8.4	-86.4 (6.4)	-20.8
54,397.65.....	0.250	70.3 (6.5)	-13.4	-144.7 (8.1)	-18.3
54,401.59.....	0.625	3.3 (5.5)	2.9	-67.6 (6.8)	-39.5
54,402.66.....	0.999	-146.3 (4.9)	-23.2	86.3 (6.0)	-31.4
54,403.68.....	0.355	96.7 (4.1)	-23.7	-179.5 (5.0)	-9.7
54,696.81.....	0.723	-79.5 (4.4)	-0.4	91.6 (5.4)	25.9
54,696.94.....	0.770	-114.9 (5.7)	-2.7	109.7 (7.0)	4.9
54,697.80.....	0.069	-81.1 (3.7)	-12.9	56.0 (4.5)	3.1
54,697.95.....	0.120	-41.3 (5.5)	-19.6	26.9 (6.8)	28.9
54,698.74.....	0.397	108.6 (5.8)	-11.4	-168.3 (7.1)	1.0
54,698.94.....	0.467	90.6 (5.6)	-11.2	-147.3 (5.6)	0.5
54,699.83.....	0.777	-125.0 (4.6)	-8.3	106.6 (5.7)	-3.7
54,700.85.....	0.135	-8.6 (26.3)	-1.8	...	...
54,701.86.....	0.488	105.8 (5.4)	13.0	-125.6 (6.7)	11.6
54,724.65.....	0.447	122.3 (3.8)	13.0	-146.6 (7.9)	10.0
54,724.75.....	0.481	103.5 (4.4)	7.6	-137.3 (5.5)	3.5
54,725.67.....	0.802	-138.8 (3.8)	-7.1	120.9 (4.7)	-6.9
54,725.77.....	0.837	-141.6 (4.3)	4.9	136.6 (5.2)	-8.8
54,726.67.....	0.151	18.0 (3.9)	10.1	-60.8 (4.9)	-23.8
54,726.77.....	0.185	35.9 (3.1)	-1.5	-83.7 (3.8)	-11.9
54,729.68.....	0.201	67.0 (3.6)	17.0	-70.7 (4.5)	15.9
54,729.74.....	0.226	86.8 (2.7)	18.3	-89.5 (3.3)	19.1
55,040.87.....	0.878	-123.0 (6.6)	33.2	179.4 (8.2)	22.6
55,041.67.....	0.155	11.9 (28.4)	0.4	...	...
55,043.67.....	0.856	-118.9 (6.8)	33.4	191.7 (8.3)	39.5
55,044.77.....	0.240	79.4 (9.0)	1.7	-107.9 (11.1)	11.5
55,045.70.....	0.565	55.6 (6.4)	9.0	-117.8 (7.9)	-35.2
55,046.68.....	0.906	-123.4 (6.1)	33.5	190.4 (7.5)	32.9

Table 2—Continued

Date (HJD-2,400,000)	$\phi$	$V_{r1}$ (km s <sup>-1</sup> )	$O_1 - C_1$ (km s <sup>-1</sup> )	$V_{r2}$ (km s <sup>-1</sup> )	$O_2 - C_2$ (km s <sup>-1</sup> )
55,047.66.....	0.250	103.3 (4.4)	19.1	-90.3 (8.9)	36.8

Table 3. Orbital Elements

Element	MT311	MT429	MT605	MT696	MT720	MT771
$P$ (Days)	5.752±0.005	2.9786±0.0001	12.27±0.01	1.4692±0.0005	4.3622±0.0003	2.8635±0.0002
$e$	0.0 (fixed)	0.0 (fixed)	0.24±0.07	0.01±0.02	0.35±0.02	0.05±0.03
$\omega$ (deg)	341±180	339±180	56±13	170±180	297±3	41±29
$\gamma$ (km s <sup>-1</sup> )	1±4	-14±1	-12±2	-10±3	-9±3	-13±2
$T_0$ (HJD-2,400,000)	52,149 (fixed)	51,784.66 (fixed)	54,653.2±0.5	54729.0±0.7	54,585.80±0.04	54,408.4±0.2
$K_1$ (km s <sup>-1</sup> )	88±5	~140	44±3	261±4	173±5	139±5
$K_2$ (km s <sup>-1</sup> )	118±9	~205	77±5	307±9	242±7	164±6
$M_1$ (M <sub>⊙</sub> )	>3.0±0.7 <sup>a</sup>	7.6	>1.3±0.3 <sup>a</sup>	>15.1±0.7 <sup>a</sup>	>15.5±0.8 <sup>a</sup>	>4.5±0.3 <sup>a</sup>
$M_2$ (M <sub>⊙</sub> )	>2.2±0.4 <sup>a</sup>	5.2	>0.7±0.1 <sup>a</sup>	>12.8±0.5 <sup>a</sup>	>11.1±0.6 <sup>a</sup>	>3.8±0.2 <sup>a</sup>
$f(m)_1$ (M <sub>⊙</sub> )	0.4±0.1	...	0.10±0.03	2.7±0.2	1.9±0.2	0.80±0.08
$f(m)_2$ (M <sub>⊙</sub> )	1.0±0.3	...	0.5±0.1	5.2±0.4	5.3±0.6	1.3±0.1
S. C. <sub>1</sub>	B2V	[B3V]	B0.5V	O9.5V	B0-1V	O7V
S. C. <sub>2</sub>	B3V	[B6V]	[B2.5:V]	B1:V	B1-2V	O9V
$a_1 \sin i$ (R <sub>⊙</sub> )	10.0±0.6	8.3	10.4±0.8	7.6±0.1	14.0±0.4	7.867±0.004
$a_2 \sin i$ (R <sub>⊙</sub> )	13.40±0.01	12.1	18.07±0.02	8.921±0.004	19.57±0.01	9.3±0.3
$rms_1$ (km s <sup>-1</sup> )	12.5	...	7.2	21.6	17.9	16.8
$rms_2$ (km s <sup>-1</sup> )	23.0	...	8.6	29.5	25.4	23.9
$i$ (°)	~42 <sup>b</sup>	89	~80 <sup>b</sup>	~26 <sup>b</sup>	~70 <sup>b</sup>	≤37 <sup>b</sup>
$T_1$ (K)	...	19,100	...	...	...	...
$T_2$ (K)	...	13,700	...	...	...	...
$R_1$ (R <sub>⊙</sub> )	...	4.8	...	...	...	...
$R_2$ (R <sub>⊙</sub> )	...	3.6	...	...	...	...

Note. — Calculated errors are located in parentheses. Square brackets indicate spectral types that have been determined indirectly from the data (i.e., based on the computed mass ratio rather than the component's spectrum).

<sup>a</sup>Calculated mass is equal to  $M \sin^3 i$ .

<sup>b</sup>Estimated based on the theoretical masses of the components' spectral types.

Table 4. Ephemeris for MT429 Spectroscopy

Date (HJD-2,400,000)	$\phi$	$V_r$ (km s <sup>-1</sup> )
51,805.89.....	0.187	0.8 (5.2)
52,146.85.....	0.658	-28.0 (4.0)
52,161.67.....	0.634	-23.1 (4.5)
52,162.84.....	0.029	-5.1 (3.9)
53,339.59.....	0.100	3.9 (5.7)
53,340.59.....	0.437	-15.5 (4.5)
53,989.78.....	0.391	-6.7 (6.6)
54,286.91.....	0.148	2.2 (7.4)
54,628.88.....	0.957	-15.9 (4.5)
54,630.85.....	0.619	-22.8 (6.2)
54,699.77.....	0.758	-32.0 (3.6)
54,700.79.....	0.099	-3.7 (12.8)
54,701.75.....	0.423	-12.7 (2.5)
55,430.90.....	0.221	4.0 (7.6)
55,497.59.....	0.612	-32.1 (6.5)

Note. — The radial velocities listed in the table reflect the radial motion of the B2V component as diluted by the (apparently constant velocity) spectrum of the brighter B0V component.

Table 5. OB Binaries in Cyg OB2

Star	Type	S.C.	P (days)	e	q	Ref.
MT059	SB1	O8V + [B]	4.8527 (0.0002)	0.11 (0.04)	0.22–0.67 <sup>a</sup>	1
MT145	SB1	O9III + [mid B]	25.140 (0.008)	0.291 (0.009)	0.26–0.63 <sup>a</sup>	2
MT252	SB2	B2III + B1V	18–19	...	0.8 (0.2)	1
MT258	SB1	O8V + [B]	14.660 (0.002)	0.03 (0.05)	0.18–0.89 <sup>a</sup>	1
MT311	SB2	B2V + B3V	5.752 (0.005)	0.0 (fixed)	0.75 (0.07)	3
MT372	SB1/EA:	B0V + [B2:V]	2.228 (fixed)	0.0 (fixed)	~0.6	2,4
MT421	SB1:/EA	O9V + [B9V–A0V]	4.161	...	~0.16–0.19	5
MT429	SB1/EA	B0V + [B3V] + [B6V]	2.9786 (0.0001)	0.0 (fixed)	~0.68	3,5,6,7
MT605	SB2	B1V + [B2.5:V]	12.27 (0.01)	0.24 (0.07)	0.57 (0.05)	3
MT696	SB2/EW/KE	O9.5V + B0V	1.4692±0.0005	0.01 (0.02)	0.85 (0.03)	3,8
MT720	SB2	B0–1V + B1–2V	4.3622 (0.0003)	0.35 (0.02)	0.71 (0.06)	1,3
MT771	SB2	O7V + O9V	2.8635 (0.0002)	0.05 (0.03)	0.85 (0.05)	1,3
Schulte 3	SB2/EA:	O6IV: + O9III	4.7464 (0.0002)	0.070 (0.009)	0.44 (0.08)	1,9
Schulte 5	SB2/EB	O7Ianf + Ofpe/WN9 (+ B0V:)	6.6 (fixed)	0.0 (fixed)	0.28 (0.02)	10,11,12,13, 14,15,16
Schulte 8a	SB2	O5.5I + O6:	21.908 (fixed)	0.24 (0.04)	0.86 (0.04)	17,18
Schulte 9	SB2	O5: + O6–7:	2.355 yr	0.708 (0.027)	0.9 (0.1)	19,20
Schulte 73	SB2	O8III + O8III	17.28 (0.03)	0.169 (0.009)	0.99 (0.02)	2
A36	SB2/EA	B0Ib + B0III	4.674 (0.004)	0.10 (0.01)	0.70 (0.06)	2,21,22
A45	SB2	B0.5V + B2–3V:	2.884 (0.001)	0.273 (0.002)	0.46 (0.02)	2,22
B17	SB2/EB:	O7: + O9:	4.0217 (0.0004)	0 (fixed)	0.75 (fixed)	23,24

Note. — Photometric types EW/KE, EA, and EB stand for eclipsing system of the W UMa type (ellipsoidal;  $P < 1$  day), Algol type (near spherical), and  $\beta$  Lyr type (ellipsoidal;  $P > 1$  day) respectively. The mass ratio for MT421 is calculated using the O star masses of Martins et al. (2005) and interpolated AB masses of Drilling & Landolt (2000). The mass ratio associated with the system composed of MT429b + MT429c has been indirectly determined from the photometric data using PHOEBE. Square brackets indicate spectral types that have been determined indirectly from the data (i.e., based on the computed mass ratio rather than the component’s spectrum).

<sup>a</sup>The range in mass ratio incorporates both observational and inclination uncertainties

References. — (1) Paper II; (2) Paper III; (3) This work; (4) Wozniak et al. (2004); (5) Pigulski & Kolaczowski (1998); (6) Cabellero-Nieves et al. (2011) (7) Henderson et al. (2011) (8) Rios & DeGioia-Eastwood (2004); (9) Kiminki & Kobulnicky (2012b, in prep); (10) Wilson (1948); (11) Wilson & Abt (1951); (12) Miczaika (1953); (13) Walborn (1973); (14) Contreras et al. (1997); (15) Rauw et al. (1999); (16) Hall (1974); (17) Romano (1969); (18) De Becker et al. (2004); (19) Nazé et al. (2008); (20) Nazé et al. (2010); (21) Otero (2008a); (22) Hanson (2003); (23) Stroud et al. (2010); (24) Otero (2008b)

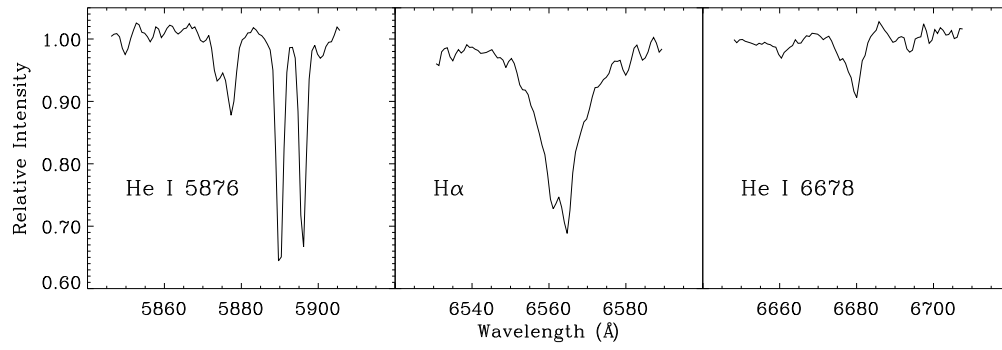


Fig. 1.— A composite of four spectra between a phase of  $\phi = 0.457$  and  $\phi = 0.655$  for MT311. The three panels show He I  $\lambda 5876$  Å, H $\alpha$ , and He I  $\lambda 6678$  Å at quadrature respectively.

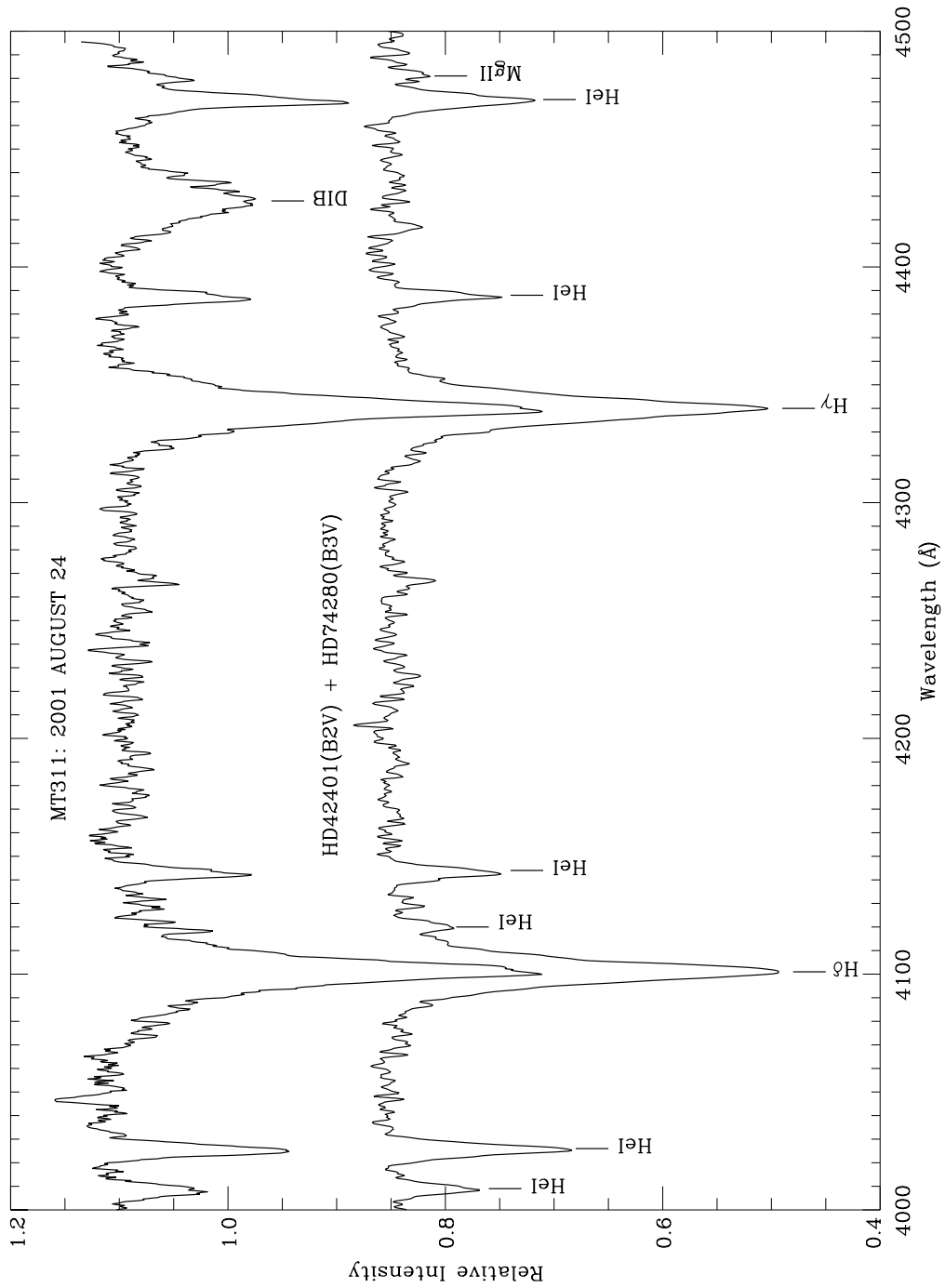


Fig. 2.— Spectrum of MT311 (top) obtained on 2001 August 24 and a composite of two spectra that best match the spectral types of the primary and secondary from the Walborn & Fitzpatrick (1990) digital atlas shifted to the appropriate radial velocities.

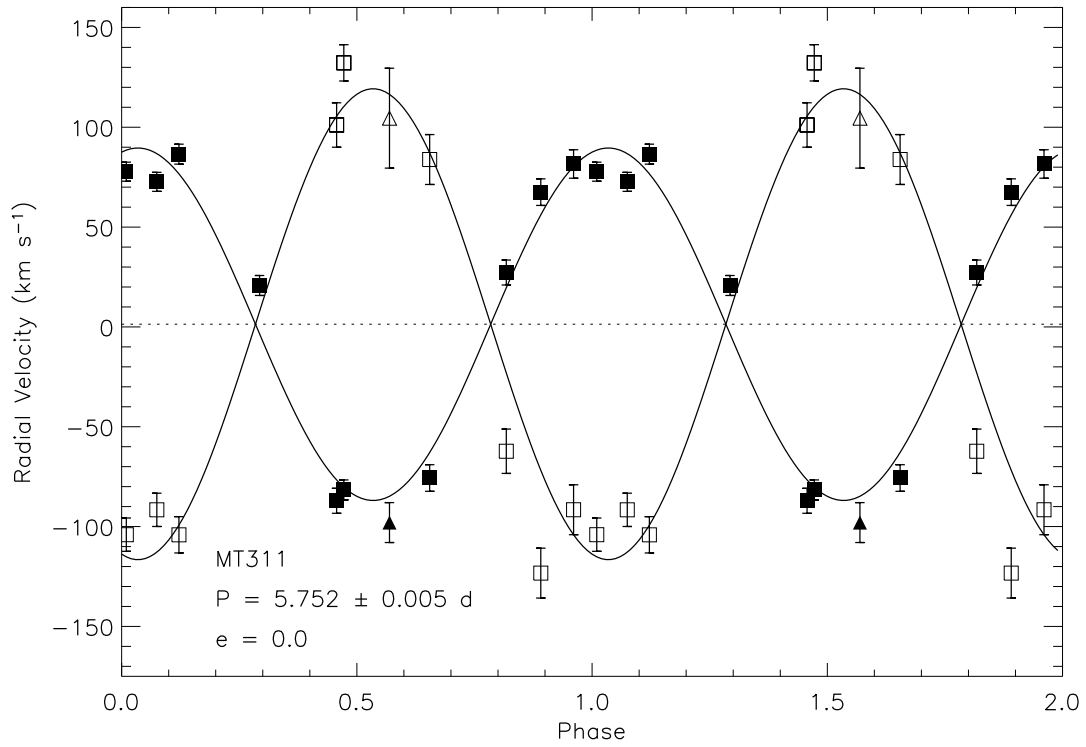


Fig. 3.— Heliocentric radial velocity curve and orbital solution for MT311 using 11 of the highest S/N spectra. The filled points correspond to the primary (B2V) and the open points correspond to the secondary (B3V). The triangle represents an observation taken with Hydra at WIYN and the squares represent observations taken with WIRO-Longslit at WIRO.

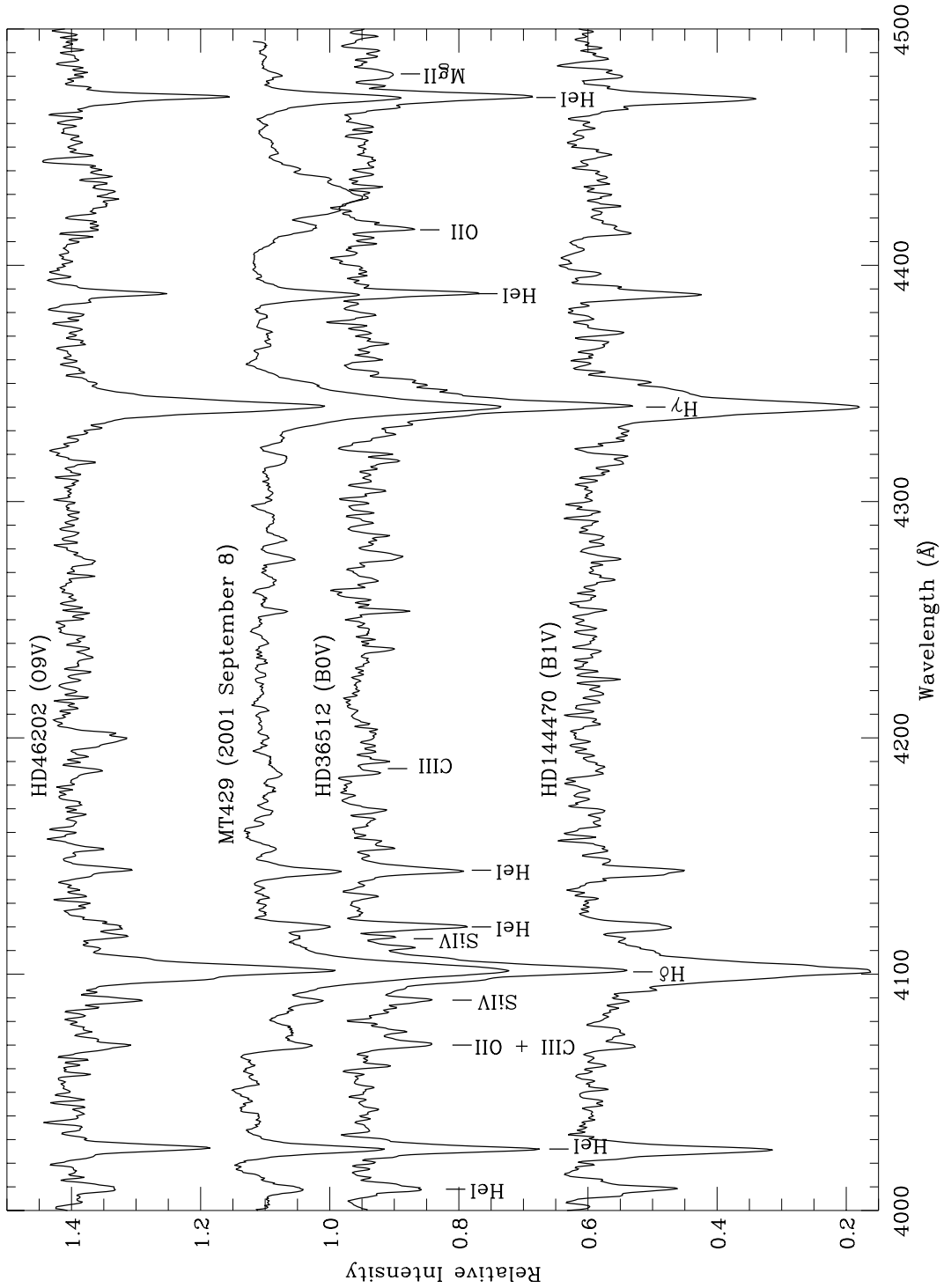


Fig. 4.— Spectrum of MT429a (second from top) obtained on 2001 September 8 and an O9V (HD46202), a B0V (HD36512), and a B1V (HD144470) from the Walborn & Fitzpatrick (1990) digital atlas for comparison.

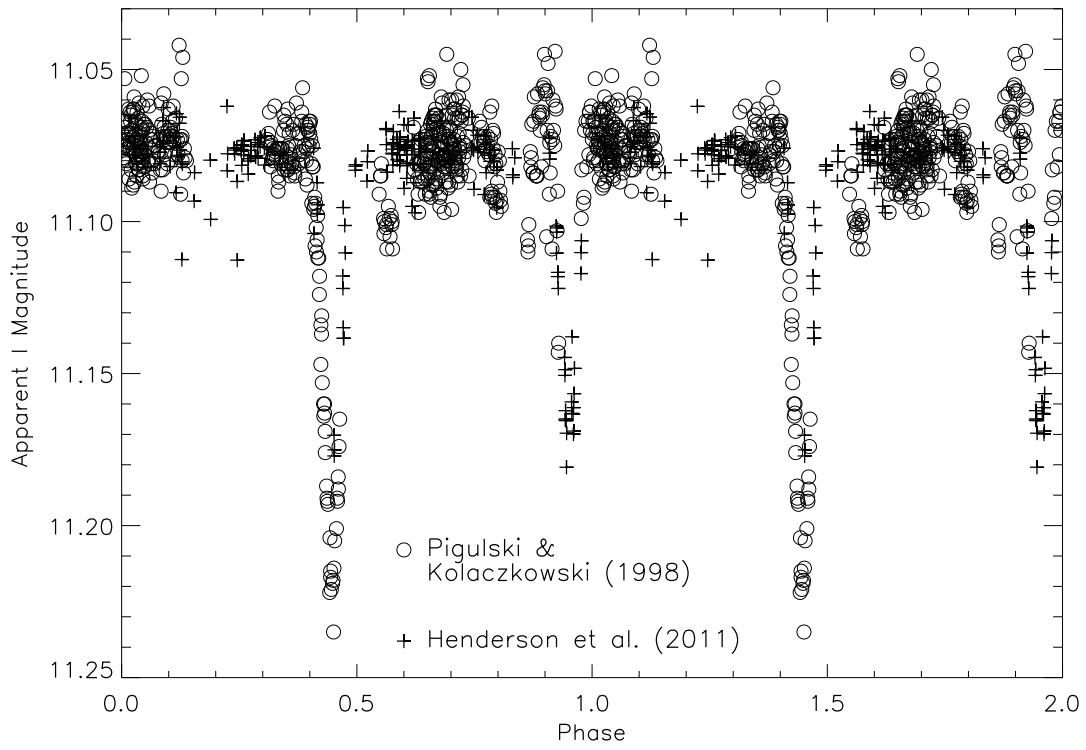


Fig. 5.— Combined I-band photometric data from Pigulski & Kolaczowski (1998) and Henderson et al. (2011) folded at a period of 2.9786 days.

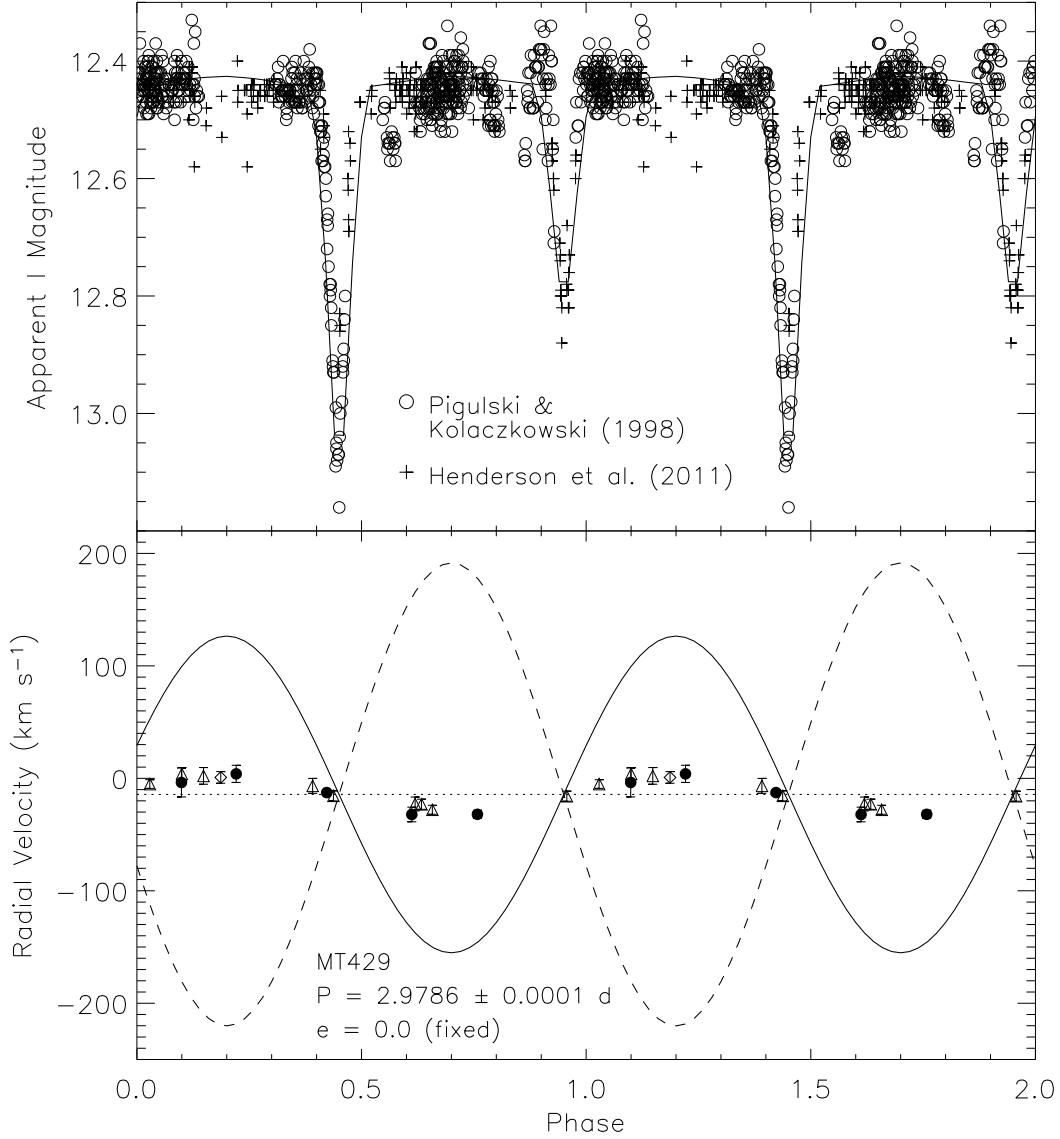


Fig. 6.— Upper panel: the I-band photometric data and best-fit PHOEBE light curve solution for MT429. Open circles are the I magnitudes obtained from Pigulski & Kolaczowski (1998), and the crosses are the I magnitudes obtained from Henderson et al. (2011) Lower panel: theoretical velocity curve for the putative B3V (solid curve) and B6V (dashed curve) components under the triple system (B0V+B3V+B6V) scenario described in the text for MT429. Data points (filled circles for WIRO, triangles for WIYN, a diamond for Keck) show the apparent observed heliocentric radial velocity in the composite spectrum which is dominated by the (presumably constant velocity) B0V modulated by the  $\sim 140$  km s<sup>-1</sup> amplitude signal of the fainter B2V.



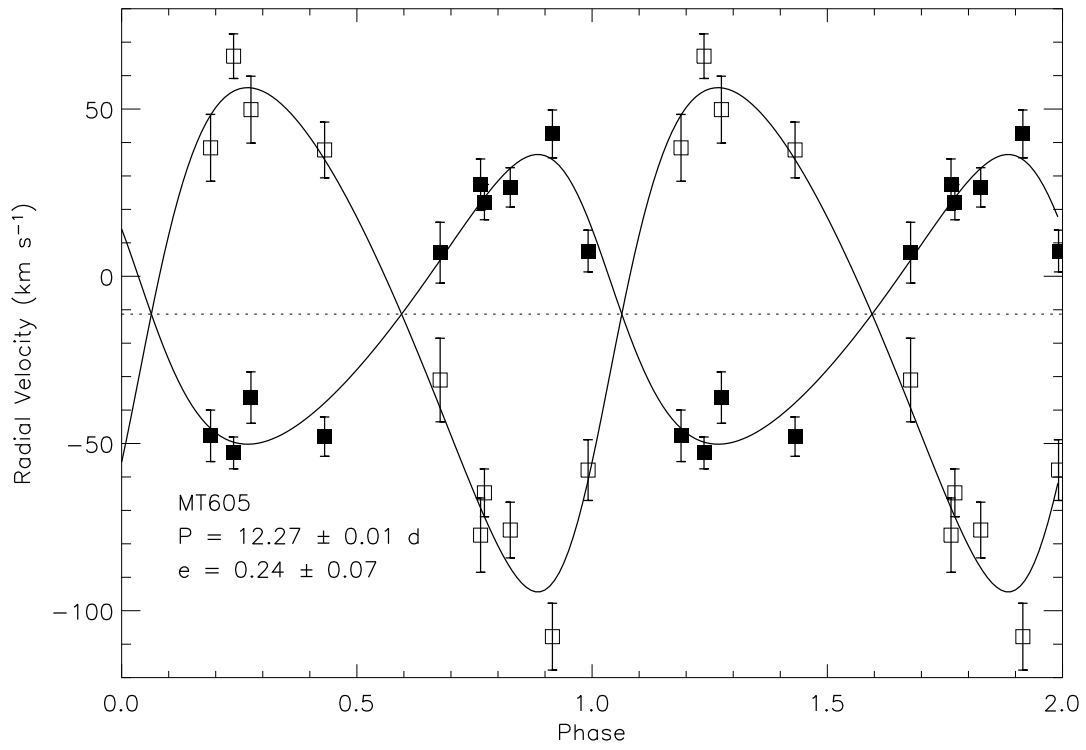


Fig. 8.— Heliocentric radial velocity curve and orbital solution for MT605 using 10 of the highest S/N spectra obtained at WIRO with WIRO-Longslit.

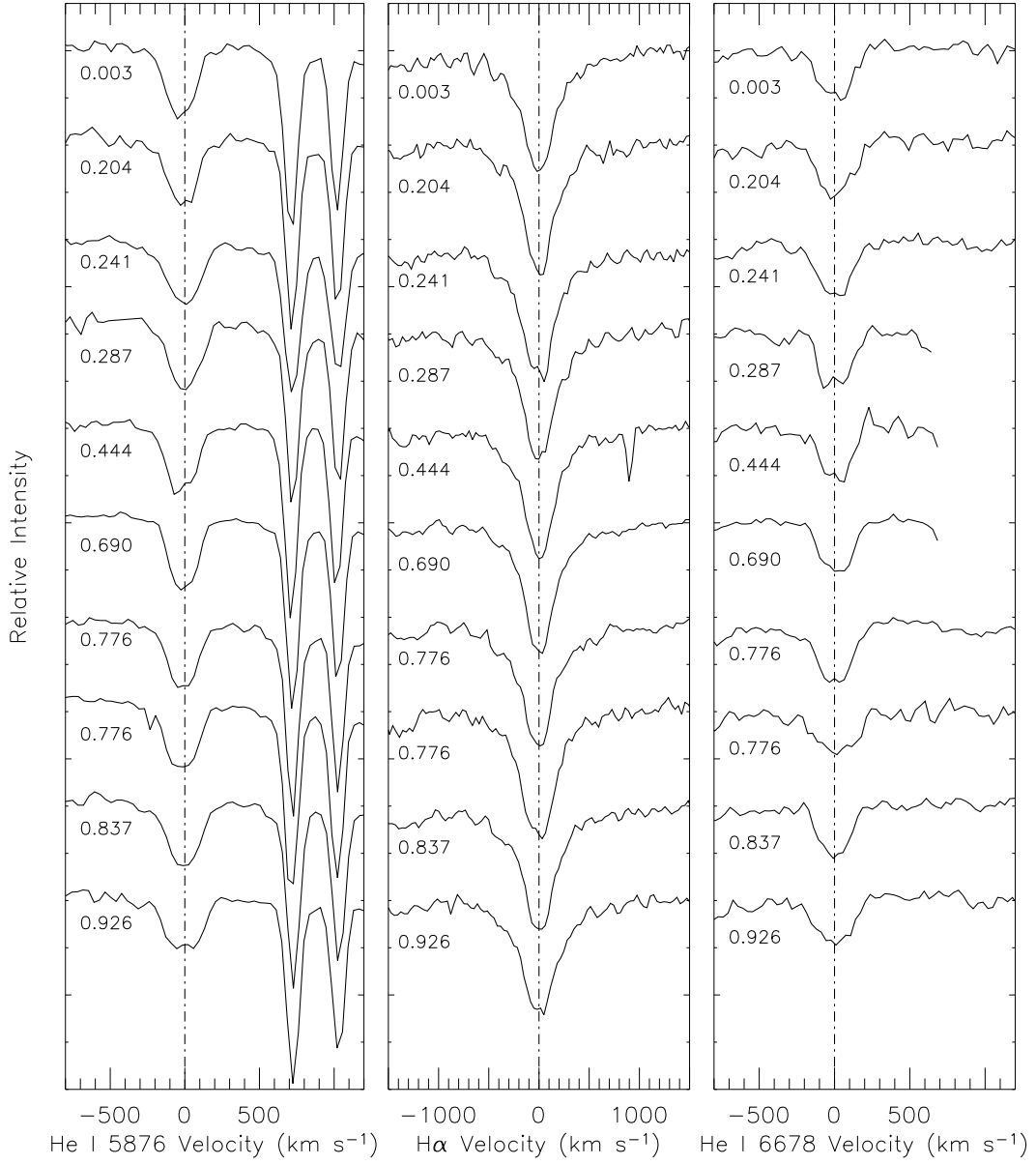


Fig. 9.— He I  $\lambda 5876$  Å (left), H $\alpha$   $\lambda 6563$  Å (middle), He I  $\lambda 6678$  Å (right) in velocity space and in order of phase for observations of MT605 taken at WIRO between 2008 June 25 and 2009 August 4.

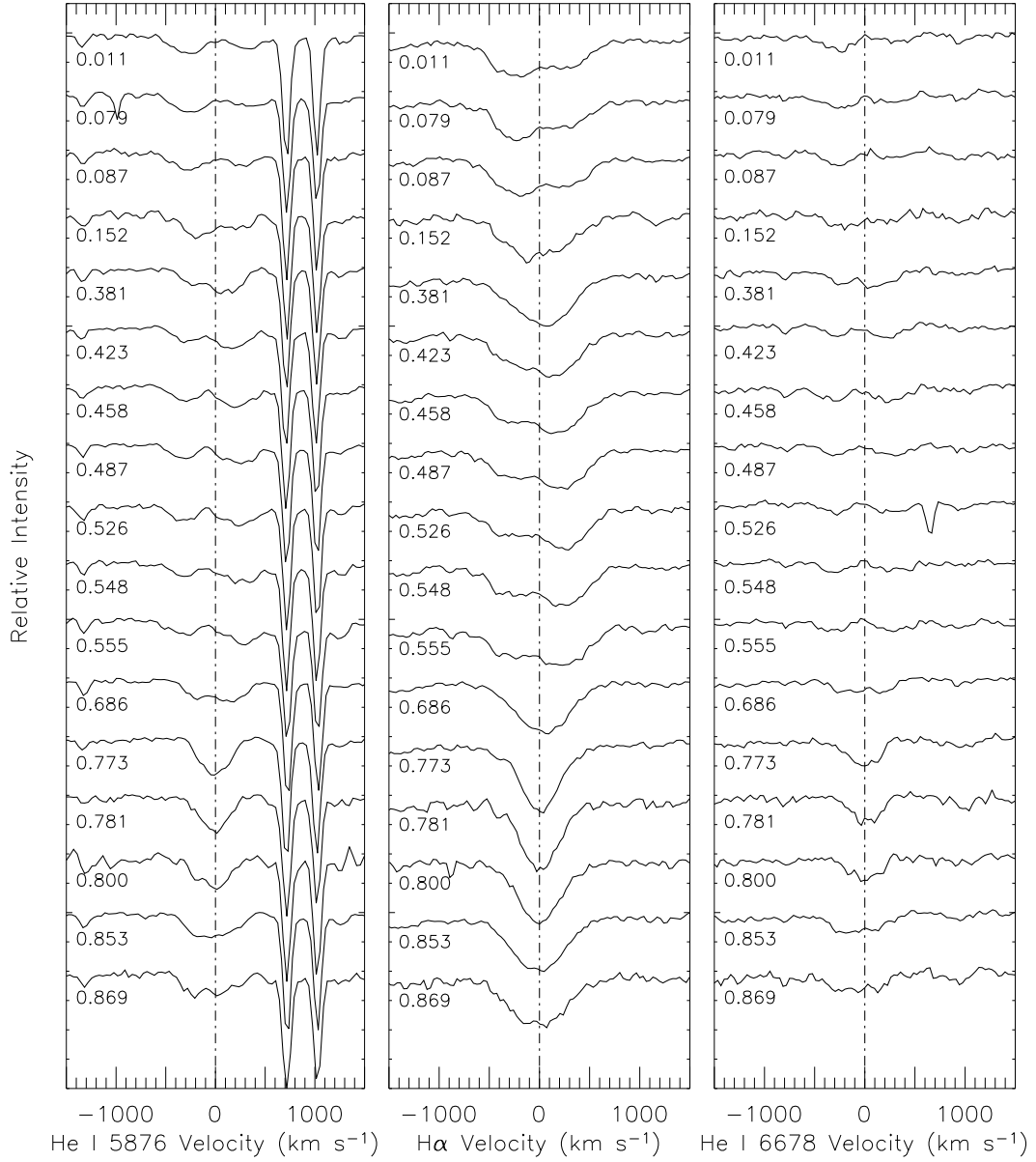


Fig. 10.— He I  $\lambda 5876$  Å (left), H $\alpha$   $\lambda 6563$  Å (middle), He I  $\lambda 6678$  Å (right) in velocity space and in order of phase for observations of MT696.

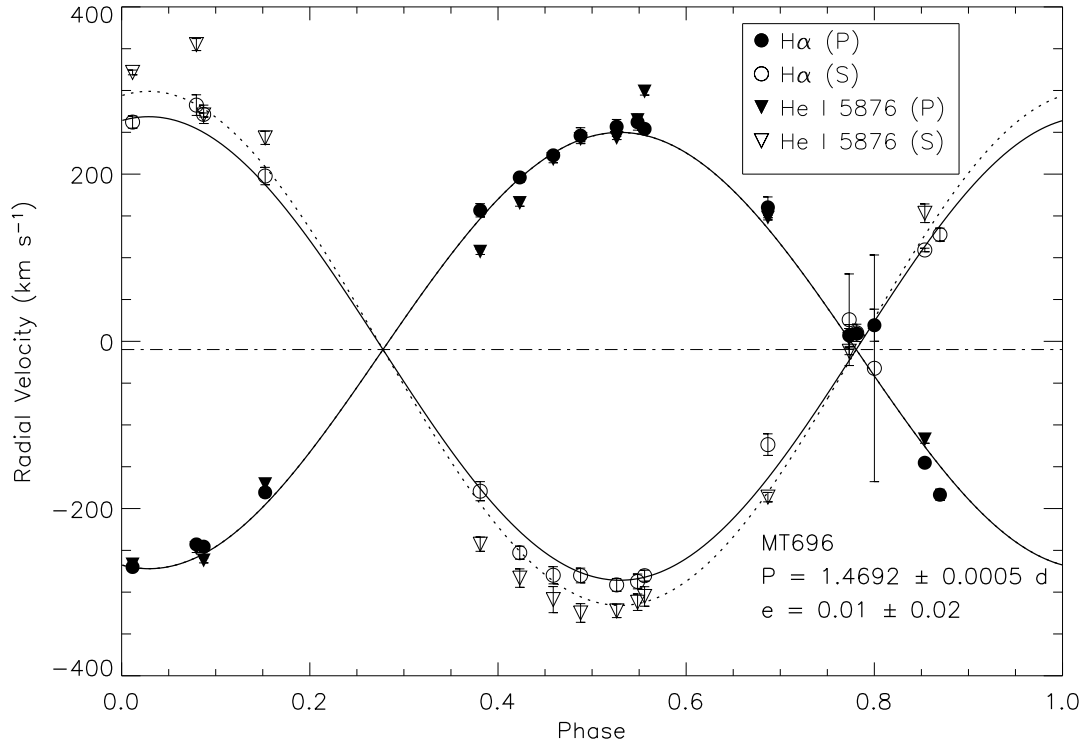


Fig. 11.— Heliocentric radial velocity curves and orbital solutions for the eclipsing binary (W Uma type), MT696 (O9.5V + B0V) using 17 spectra obtained at WIRO with WIRO-Longslit. The circles and solid line represent the velocities and orbital solution obtained from H $\alpha$  and the triangles and dotted line represent the velocities and orbital solution obtained from He I  $\lambda$ 5876 Å. Filled and open symbols correspond to the primary and secondary respectively.

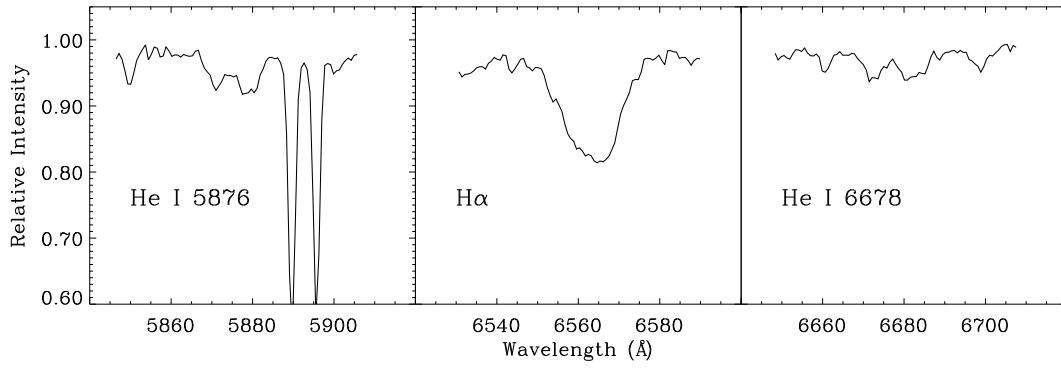


Fig. 12.— A composite of seven spectra between a phase of  $\phi = 0.5$  and  $\phi = 0.7$  for MT720. The three panels show He I  $\lambda 5876$  Å, H $\alpha$ , and He I  $\lambda 6678$  Å at quadrature respectively.

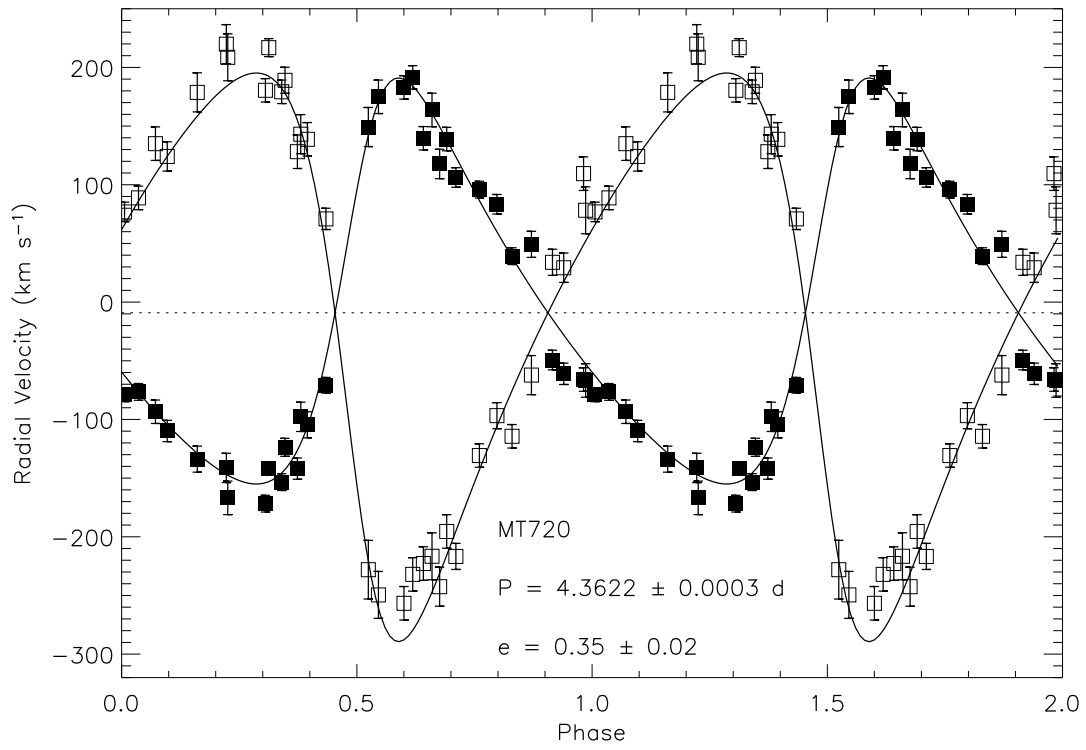


Fig. 13.— Heliocentric radial velocity curve and orbital solution for MT720 using 32 of the highest S/N spectra obtained at WIRO with WIRO-Longslit.

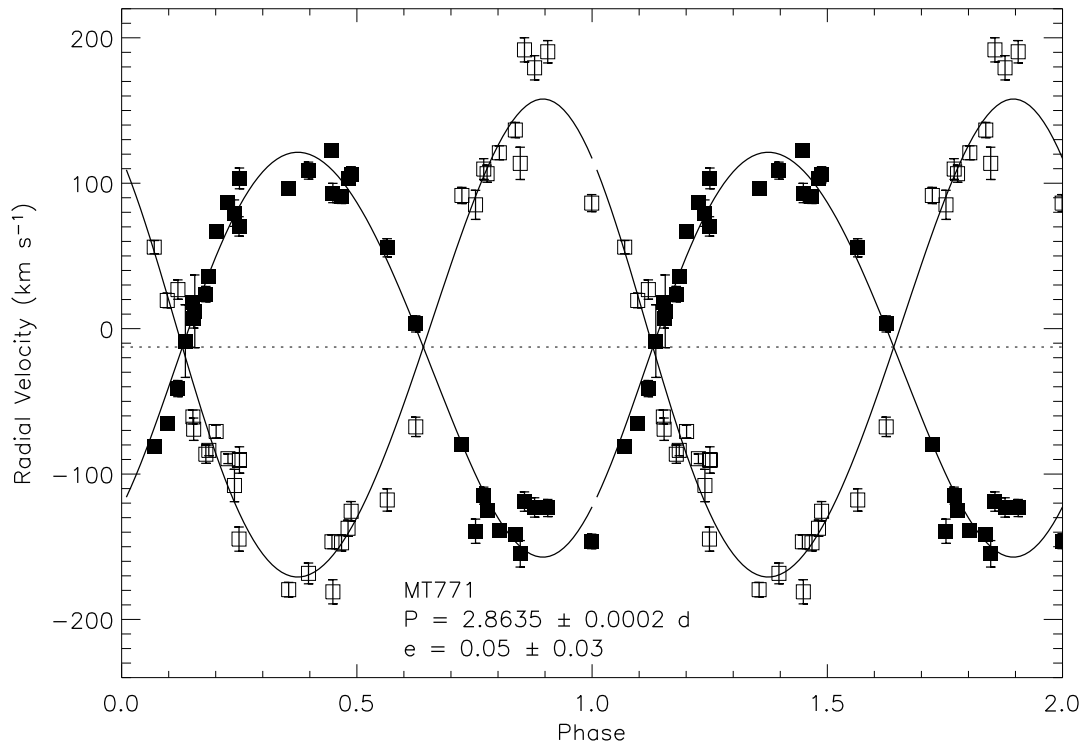


Fig. 14.— Heliocentric radial velocity curve and orbital solution for MT771 using 34 of the highest S/N spectra obtained at WIRO with WIRO-Longslit.

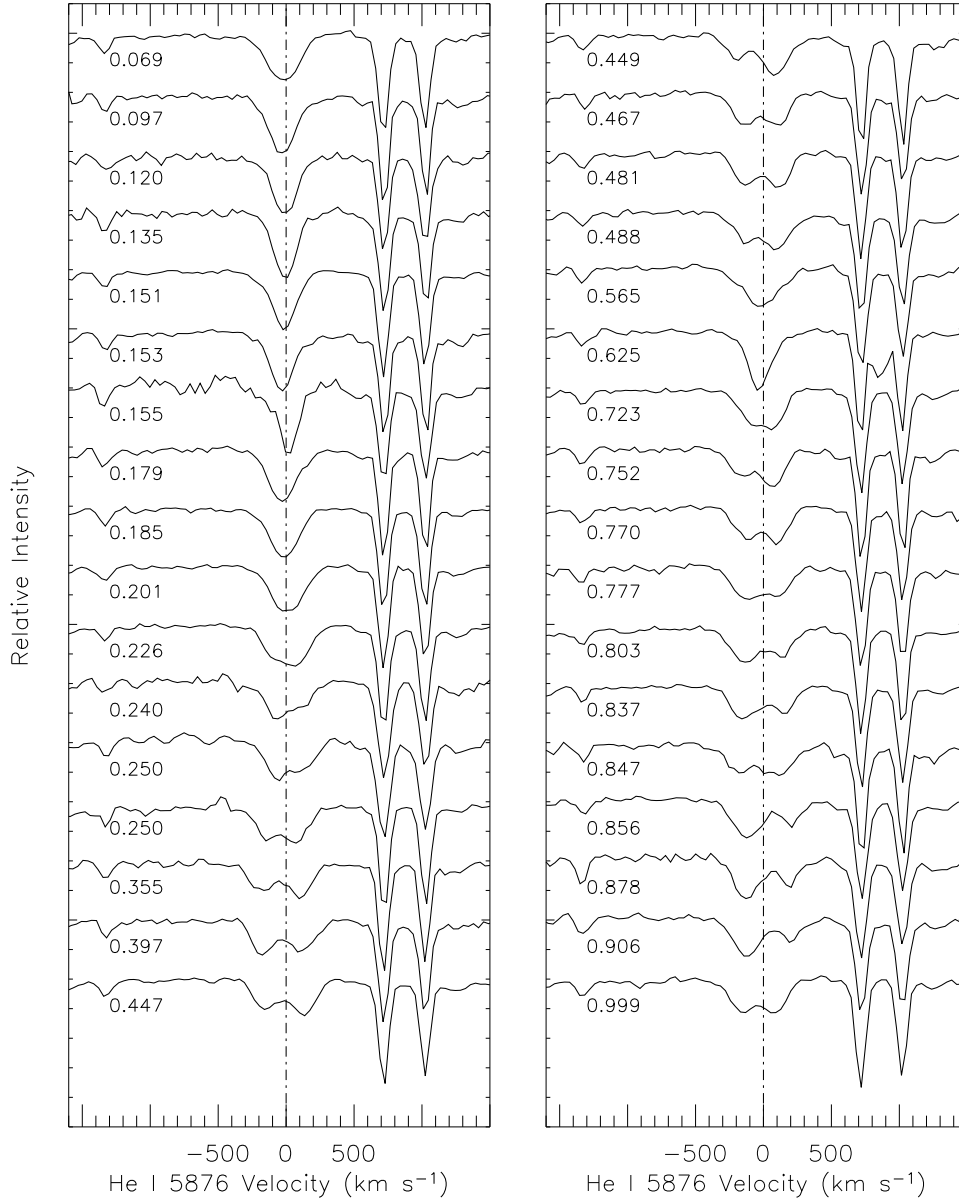


Fig. 15.— He I  $\lambda 5876$  Å in velocity space and in order of phase for observations of MT771 obtained at WIRO with WIRO-Longslit from 2007–2009.

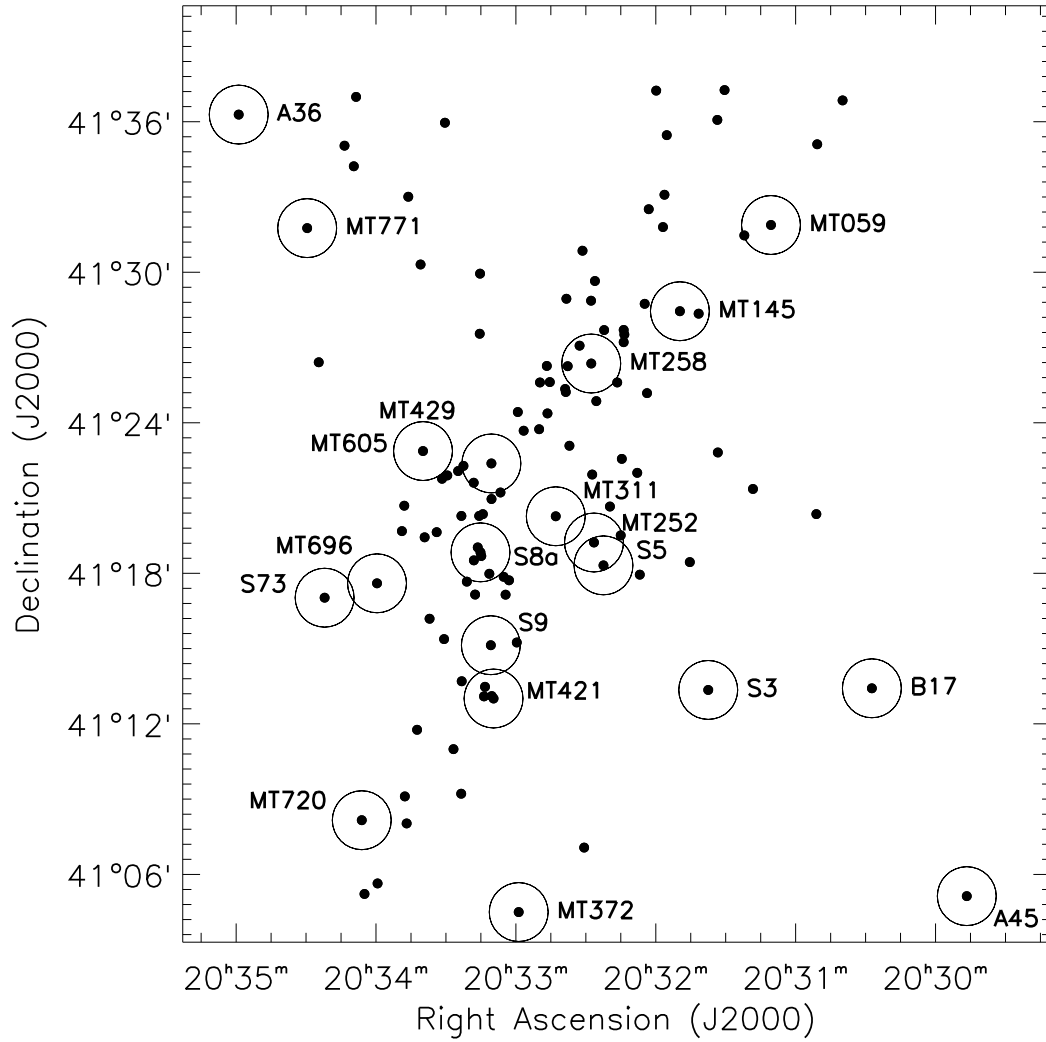


Fig. 16.— Map of OB stars in Cyg OB2. Circles indicate the location of the 20 known binaries within Cyg OB2. We find no apparent clusterings or groups of massive stars, nor a tendency for them to be located near the center of the Association.